VON KARMAN INSTITUTE FOR FLUID DYNAMICS
CHAUSSEE DE WATERLOO, 72
B - 1640 RHODE SAINT GENESE, BELGIUM

PROJECT REPORT 1981-19 JUNE 1981

HEAT TRANSFER ON THE ENDWALL OF A TURBINE CASCADE WITH FILM COOLING

ABDULLAH ÖNGÖREN

SUPERVISORS : P. LIGRANI
C. CAMCI

ACKNOWLEDGEMENT

I am indebted to Dr. Ph. Ligrani, VKI Assistant Professor, and Mr. C. Camci, VKI Doctoral Candidate, for their continuous help and encouragement during this study.

I express my thanks to Mr. C.H. Sieverding, VKI Associate Professor, for his valuable discussions about blade passage hydrodynamics. My thanks are also due to Mr. R. Conniasselle and Mr. F. Vande Broeck, laboratory staff at VKI, for their help in the preparation of experiments.

ABSTRACT

The results of an investigation of the heat transfer on film cooled turbine endwall are presented. The effect of secondary flows and cooling injection rates on endwall heat transfer are investigated. A comparison with measurements is provided using results of experiments from a flat plate having the same favorable pressure gradient and the same downstream injection locations. A two-dimensional mixing-length prediction scheme and it's modified version applicable to film cooling predictions are also used for comparison with measurements.

A good match of predictions and measurements are observed in case of no injection. The predictions and measurements are in qualitative agreement in the existance of film cooling. It is also found that the endwall secondary flows cause non-uniform distributions of film cooling injectant resulting in varying heat transfer rates across the width of the blade passage. The effect of injection rates on heat transfer is evident: low heat transfer is observed at high injection rates. The heat transfer measured on the center streamline of the endwall with film cooling shows qualitative agreement with flat plate results.

TABLE OF CONTENTS

NOMENCLATURE

A_c	Total injection area
A_p	Blade passage area
A_t	Compression tube area
A^+	Viscous sublayer thickness
A^*	Sonic orifice area
b	Blockage factor
c	Chord length
C_D	Discharge coefficient
C_p	Specific heat at constant pressure
C_v	Specific heat at constant volume
D	Sonic orifice diameter
h	Heat transfer coefficient
h_b	Blade height
k	Ratio of specific heats, c_p/c_v
l_1	Total length of compression tube
l_2	Displacement of compression tube piston
M	Blowing ratio, $\rho_c u_c / \rho_\infty u_\infty$
$\dot{m}_c$	Injection mass flow rate, $\rho_c u_c A_c$
$\dot{m}_p$	Cascade mass flow rate, $\rho_p u_p A_p$
Ma	Mach number
Ma_1	Inlet Mach number
Ma_2	Exit Mach number
n	number of blades
Nu	Nusselt number

P Local pressure

P_o Test section freestream total pressure

P_{oc} Plenum chamber total pressure

P_p Blade passage pressure

P Freestream static pressure

Q Endwall heat flux

R Gas constant

Re Reynolds number

Re_{δ_2} Momentum thickness Reynolds number

s Meridional coordinate

St Stanton number, $h/\rho_\infty u_\infty C_p$

t Compression time

T_c Coolant temperature

T_o Test section freestream total temperature

T_{oc} Total coolant temperature

u_c Injection velosity

u_p Piston velocity

u Freestream velocity

u' Fluctuating component of velocity in longitudinal direction

x Longitudinal coordinate

ω Plenum chamber pressure to freestream total pressure ratio

κ von Karman constant

ρ Density

ρ_∞ Freestream density

ρ_c Coolant density

ρ_p Density in the blade passage

θ Non-dimensional coolant temperature

LIST OF FIGURES

LIST OF PHOTOGRAPHS

LIST OF TABLES

1. INTRODUCTION

Because of increasing fuel costs, one of the main problems in today's gas turbine design is to find means to increase thermal efficiency and specific power. Designing low aspect ratio turbines is one solution. However turbine inlet temperature may also be increased to obtain high thermal efficiency and specific power.

High turbine inlet temperatures are restricted with ultimate strengths and melting points of turbine component materials since they result in high thermal stresses in components. These stresses may cause direct failure or result in low cycle fatique and creep failure. Although cooled turbines appear to be a convenient solution, even with cooled components, the temperatures of present materials may not exceed 1200 °C. This limit is lower in uncooled solid blades and endwalls.

Cooling means losses in turbine efficiency since it increases the drag on cooled surfaces and creates entropy increase and pressure loss in the flow. Cooled components designed for high turbine inlet temperatures also have complex geometries which are difficult to manufacture. To keep the inlet temperature as high as possible and to minimize the losses due to cooling air, the heat transfer distributions on and within components are needed.

The turbine endwall is one component where local heat loads must be known precisely in order to design a turbine with high inlet temperature. Because of the complex flow behaviour near an endwall accurate calculation of heat transfer rates is not presently possible. The complicated behaviour of near-wall flow is due to the existance of strong secondary flows in this region. The studies in stationary turbine cascades show that these flows are in the form of passage vortex, counter vortex, corner vortex, and crossflow as well as boundary layer skewness and three-dimensional separation. The near-wall flow inside a passage is highly three-dimensional and complicated in the

vicinity of these flows. In cases where film or transpiration cooling is used, the effect of injected fluid on secondary flows should also be considered. Such flows may increase or decrease the effect of secondary flows depending upon the rate of injection and its interaction with the surrounding flow field (Sieverding (1985)

The related studies in the literature show that heat transfer to an endwall is strongly affected by secondary flow development. This feature of endwall heat transfer has been illustrated by Blair (1971) and Graziani (1980) quantitatively. The quantitative results given by Blair and Graziani to show the effect of secondary flows on endwall heat transfer were obtained on a large scale turbine vane passage placed in a wind tunnel. With such configurations it is possible that the secondary flow mechanisms are different than those which exist in a real turbine cascade. This is supported by the conclusions from the studies that secondary flows are dependent on geometry as well as on flow conditions. In addition, the experimental set up used by Blair and Graziani ignores blade periodicity. Only in the Blair study are secondary flows investigated in the vicinity of cooling. In his study Blair used a slanted injection slot located at the inlet of the blade passage. This geometry is not adequate in real turbine applications due to strength problems.

The main purpose of the present work is to investigate the effect of film cooling injection on endwall heat transfer as the injection flow rate varies. Reynolds number, Re, Mach number, Ma, and freestream/coolant temperature ratio of a typical cooled gas turbine are to be simulated in the test section.

A small scale turbine cascade with double row of slanted discrete hole injection at three locations is used for the present study. Six blades on the cascade provide some periodicity of the flow. The development of secondary flows is believed to be similar to that of a typical turbine without rotational or annular effects.

A series of flat plate measurements were taken on a set-up having favorable flow conditions as the turbine cascade in order to use them in the investigation of the effect of three-dimensionality on endwall heat transfer. Comparison of the turbine endwall heat transfer measurements taken along the center streamline with two-dimensional flat plate measurements are then made. Predictions of flat plate measurements with and without cooling are also contained in this study.

2. LITERATURE REVIEW

Numerous studies have been concerned with the mechanisms of secondary flows in cascades witout heat transfer. In this report only the ones that are closely related to endwall heat transfer will be mentioned. Among these studies, Dring and Booth attempt an analytical solution to describe secondary flows in cascades, Langston explaines secondary flow mechanisms qualitatively and Sieverding and Wilputte give the effect of secondary injection on blade losses.

Dring (1971) has worked on a momentum integral analysis of the three-dimensional turbine endwall boundary layer.In this study the momentum integral approach has been refined to suit a turbine endwall boundary layer assuming that strong crossflow exists. The existing boundary layer is assumed to be incompressible, three-dimensional and turbulent. The solution obtained by Dring gives the distribution of the boundary layer thickness and skewness over the endwall as well as the amount of total pressure deficit of the flow leaving the endwall at the suction surface corner.

Another study on the analysis of the turbulent endwall boundary layer has been done by Booth (1975). In contrast to Dring, Booth does not assume incompressibility. In this study an aerodynamic loss model is derived and predictions for some cascade tests are given. In addition, Booth has investigated the effect of inlet boundary layer thickness and blade height to blade chord ratio on losses and heat transfer. He has found that secondary losses are proportional to inlet boundary layer thickness to blade height ratio.

Secondary flows in cascades have been investigated on qualitative basis by Langston et al. (1977) and by Langston (1980). In the first of these studies the authors present an experimental study of three-dimensional flow in a turbine cascade in which particular attention is devoted to endwall flows.Due to detailed measurements of subsonic flow in a large-scale plane

turbine cascade, it is shown that three-dimensinal seperation is an important feature of endwall flow. In the later study, Lanston (1980) concludes that the endwall boundary layer is characterized by small crossflows near the pressure side of the passage and large crossflows near the suction side. He also conludes that the crossflow data shows a Johnston triangular polar plot behaviour near the pressure side where crossflows are expected to be small.A crossover crossflow polar plot behaviour exists which is due to skewed main flow upstream on the suction side of the passage. The streamwise flow is found not to be similar to a two-dimensional boundary layer flow. Based on a correlation of the flow angle deviation data, an emprical crossflow model for endwall flow in a turbine cascade is also given.

The three-dimensional flow development through a straight cascade has been investigated by Sieverding and Wilputte (1977) by utilizing both flow visualisation and pressure probe measurements. They have presented the results to show the effect of Mach number and endwall cooling on secondary flows in a turbine cascade. As a result, they conclude that secondary flows are highly Mach number dependent and secondary flow losses increase with increasing outlet Mach number. Secondary flow effects decrease in magnitude in cases where coolant mass flow rates are high.

In contrast to the large amount of aerodynamic information available in the literature, documentation of the effect of turbine passage secondary flows on heat transfer is scarce. To the best information of the present author, the only study of endwall heat transfer as affected by film cooling has been made by Blair (1971). This study is also the earliest publication known to the present authors which is concerned with turbine endwalls.

In this study Blair has measured the film cooling effectiveness and convective heat transfer coefficient on the endwall of a large scale turbine vane passage, where the test models simulated the passage geometry and upstream cooling slot geometry of a typical first stage turbine.As a result, he has observed the influence of secondary flows on endwall heat

transfer and found that heat transfer coefficient is higher in the regions where the horseshoe vortex is present compared to neighboring regions.

Another important study of turbine endwall heat transfer was done by Louis,et al. (1974). Short duration studies of heat transfer and film cooling effectiveness were made in which flow and temperature were the same as during turbine operating conditions. The authors have shown analytically that strong secondary flow and centrifugal effects increase Nusselt number,Nu, over the level associated with one-dimensional convective heat transfer for a turbulent flow at the shroud of a turbine rotor.

An experimental study of the iso-heat transfer rate contours on the endwall of a turbine cascade was made by Georgiou et al. (1979). The authors simulated typical Mach and Reynolds number,temperature ratio as well as the blade section of a modern cooled turbine. The study includes the effect of the free-stream turbulence level and inlet boundary layer. The distribution of various heat transfer parameters like wall heat flux and Stanton numbers along streamlines are also presented. According to the results obtained by the authors, an increase in free-stream turbulence level and a decrease in inlet boundary layer thickness result in increased heat transfer rates. The authors also say that large pitchwise heat transfer gradients exist which can be attributed to secondary flows.

A recent study done by Graziani *et al.* (1980) includes the measurements of local rates of heat transfer on the endwall and on the suction and pressure surfaces of a large scale turbine blade cascade. The effect of inlet boundary layer thickness on endwall heat transfer for typical Reynolds numbers are investigated. The local variations of heat transfer associated with distinct flow regimes and regimes of strong three-dimensional flow are revealed and the dominant role of the passage vortex in determining heat transfer on the endwall and in certain regions of the airfoil surface are illustrated in this study. In summary, the results show that the Stanton number contours for thin inlet boundary layer are lower than for thicker inlet boundary layer. High heat transfer gradients are present in the vicinity of passage vortices.

3. BLADE PASSAGE HYDRODYNAMICS

Secondary flow behaviour near the endwall of a turbine cascade is dependent on many factors including geometry and free-stream flow conditions. In this study, some flow visualisation photographs of similar geometry and favorable flow conditions are used to describe the secondary flows in the cascade model. model. The first photograph is shown in Fig.1. It shows endwall flows in a turbine cascade having the same geometry as was used in this study. This photograph is from Ref. 16. The exit velocity for this case is given as 275 m/sec in the reference.

Fig.2 is also a flow visualisation photograph giving various aspects of endwall flows.The blade profile and the cascade geometry used in this visualisation are different than the present cascade model but this visualisation contains all flow mechanisms that are expected to occur in a turbine cascade.The mechanisms are described on the figure.

Fig.3 is the graph sketched from Fig.1 and Fig.2 illustrating all flow mechanisms that are believed to exist in the test model. The figures on the graph were exaggerated to illustrate them clearly. For example, in reality the inlet boundary layer is not so thick and the passage vortex passes the blade passage by rolling two or three times.

In the cascade flow, inlet boundary layer approaching the blade passage seperates and one part of it forms the crossflow at the passage inlet. The other part forms the horseshoe vortex. One leg of this vortex moves from the leading edge of one blade towards the suction surface of the opposite blade. This leg is called the passage vortex. The other leg moves on the endwall near the suction surface first. Then it lifts off the endwall and moves on the blade itself. The intersection point of endwall separation line of horseshoe vortex and attachment line of inlet boundary layer is the saddle point where all components of shear

stress are zero. In the passage another crossflow region takes place. This flow is due to the movement of low momentum fluid near the pressure side of one blade towards the suction side of the opposite one because of the pressure gradient existing between these two regions. Also in the blade passage there may be a corner vortex which starts from the region where counter vortex lifts off the endwall. It rolls in the opposite sense of passage vortex and it moves in the suction side corner of the blades towards the trailing edge.

4. EXPERIMENTAL TECHNIQUE

The VKI CT-2 test facility was used for the present study. This facility consists of a light piston contained within a compression tube. The piston is moved by the compressed air behind it. The piston moving towards the test section compresses the air isentropically. After sufficient compression the diaffer valve is opened and the flow moves through the test section. The compression time is calculated according to the required flow conditions. The calculations for the present test program is given in Appendix A. In this facility, small amounts of energy are required to achieve typical turbine conditions since it operates for a fraction of a second during a test.

The compression tube is five meters long and has a diameter of one meter. The test section connected to the tube is 0.25 by 0.10 meter. The test section Mach number, total pressure and total temperature are adjusted to required values by adjusting the pressure in the tube prior to compression and the pressure inside a dump tank which is located downstream of the test section. The dump tank volume is five cubic meters. In the facility available total temperature range is 290 °K to 600 °K and maximum allowable total pressure is seven bars.

For the heat transfer measurements thin-film platinium resistance thermometer gages are used. The detailed information about this kind of gages and their application are given in references 4 and 18. There are sixty eight heat transfer gages twenty five of which are located on 3.2 mm diameter quartz rods. Fourty three of them are on quartz inserts. Sensing parts of gages are approximately 0.5 mm wide and 3 mm long on quartz inserts and 1.5 mm wide and 3 mm long on quartz rods. The resistances of the gages range from 60 to 110 ohms.

The orientation of heat transfer gages on two quartz inserts was made utilizing a flow visualisation photograph. The locations of the gages were chosen to provide resolution of the effect of secondary flows on endwall heat transfer. The visualisation photograph which has been

taken under similar flow conditions and with the same cascade geometry was taken from Ref. 15.The streamlines existing on the photograph are believed to be similar in the present cascade model.

Twelve gages were painted along the center streamline whose location has been determined by Martensen method. This streamline is number four on Fig.8. The numbers of these gages as given in Fig.5 are 24,22,18,13,12,4,42,41,38,35,32,29. The rest of the gages on the inserts were oriented taking the visualisation photograph into consideration.They were located along the endwall streamlines existing on the photograph.The detailed gage configurations are given in figures 5,6, and 7.

In the experiments where cooling takes place, injection is made at three locations through double rows of slanted injection holes. The geometry of the injection locations is shown in Fig.5. The injection hole diameter is 0.5 mm, spanwise pitch is 1 mm, longitudinal pitch is 1.5 mm and slant angle is 30°. Injection is supplied into the main stream from a plenum chamber. The injection rate is controlled by utilizing a sonic orifice located on the supply pipe. Obtaining different injection rates at three injection locations is also possible if plenum chamber bleeds are included in the injection system. In the present test program the bleeds were kept closed. Injection temperature can be adjusted in the range from 250 °K to 600 °K.The maximum blowing ratio is 2.5 in this system.

The principles of injection system design are explained in detail in Ref. 4. The injection system calculations of the present test program are given in Appendix B.

CT-2 facility is used in connection with a data acquisition system. In this system, the data taken in the test section is transferred to the analoque circuits first and then amplified to be fed into analoque to digital converter units. The digitized data is sent to the mini computer PDP-11 for later reduction, The measurement chain and heat transfer calculation procedure is the same as Ref. 4. There are 48 channels for data acquisition with a total sampling frequency for all channels of 500 kiloherz. In the present experiments sampling frequency was 1250 herz per channel. Testing time was 524 milliseconds.

5. TEST PROGRAM

In this study, for the endwall measurements a cascade composed of six blades and mounted on a flat endwall was used. The blades has been manufactured according to the geometry of the hub section of a rotor blade designed by NASA, Ref. 21. The cascade geometry is as follows :

chord length = c = 60 mm
pitch/chord ratio = g/c = 0.725
stagger angle = = -42.5°
inlet flow angle = = 0°
blade height = h = 90 mm

For the flat plate measurements the set-up shown in Fig.4 was used. In order to be consistant with flow in a cascade a favorable pressure gradient was created in the test section by means of a contoured upper wall. The comparison of the pressure distribution on the flat plate and the pressure distribution in the cascade used is shown in Fig.8.

In both test cases, test section conditions were adjusted to suit to typical real turbine conditions. The parameters used are Mach number, total pressure and temperature of the main flow and coolant injection rate and temperature ratio. In both test cases inlet and outlet Mach numbers were approximately the same. These values are typical of operating subsonic turbines.

In the tests with cooling 0.96,1.00, and 1.15 were the blowing ratios. The non-dimensional temperature parameter, θ, was approximately 0.96 in all cases, which corresponds to total coolant temperature of 293 °K. In the tests freestream temperature varied from 388 °K to 400 °K. The freestream total pressures ranged between 2.563 and 2.553 bars. The reservoir supply pressure was in the range from 85 to 90 bars. The static pressure at the inlet of the cascade ranged from 2.335 to 2.436 bars. At the cascade exit the

measured pressures were 1.605 and 1.654 bars to obtain an exit Mach number of 0.785.

During all experiments the dump tank was kept closed to the atmosphere. Therefore the dump tank pressure and the exit pressure were not constant during a given test period. This was monitored and recorded by means of an oscilloscope. The appropriate exit pressure was marked on the photograph taken and the inlet and plenum chamber pressures corresponding to this value were used in the calculations. Injection supply pressure was adjusted to be 22,10, and 4.5 bars to obtain blowing ratios of 1.15, 1.00, and 0.96. The test conditions are given in Table 1.

TABLE 1

RUN NO.	Ma_1	Ma_2	Tu_∞ %	M	θ	P_{amb} mm Hg	T_{amb} °K	P_o mm Hg
DDD 178	0.325	0.785	0.8	1.000	0.960	757.7	292.7	1915.0
DDD 179	0.325	0.785	0.8	1.130	0.960	757.7	292.7	I915.0
DDD 180	0.325	0.785	0.8	0.960	0.960	757.7	292.7	1915.0
DDD 181	0.294	0.785	0.8	1.155	0.960	765.0	291.5	1922.4
DDD 182	0.336	0.785	0.8	1.155	0.960	765.0	291.5	1922.4
DDD 183	0.356	0.785	0.8	1.030	0.960	765.0	291.5	1922.4
DDD 184	0.356	0.785	0.8	0.980	0.960	765.0	291.5	1922.4
DDD 185	0.356	0.785	0.8	-	-	765.0	291.5	1922.4
DDD 186	0.372	0.785	0.8	-	-	765.0	291.5	1922.4

6. PREDICTION TECHNIQUE

MARTENSEN METHOD :

An extended version of the calculation method, Ref.19, was used to predict the positions of potential flow streamlines through the turbine blade pass.ge. Compressibility is taken into account in the two dimensional scheme. Output from the program includes streamline positions with corresponding Mach number distributions for given cascade geometry and inlet flow conditions.

The streamline positions and Mach number distributions for the cascade used in this project are shown in Fig.8. Streamline number four along the centerline of the passage was used to determine heat transfer gage orientation. The Mach number distributions were used to check the compatibility of flat plate and cascade freestream velocity variations with downstream distance.

STAN5 :

One of the two tools used to predict two-dimensional boundary layer flows is STAN5. STAN5 was developed by Crawford et al.(1976) utilizing a procedure established by Patankar and Spalding (1970). The program is suitable for two-dimensional calculation of boundary layers on a flat plate, flow inside nozzles and diffusers, flow over axis-symmetric bodies, and fully developed flow inside circular pipes and flat ducts. Here this program is used to calculate two-dimensional flow on a flat plate.

The STAN5 program solves the momentum equation of the boundary layer and any number of diffusion equations simultaneously. The boundary layer may be either laminar or turbulent where transition can also be included. The criteria used for transition is set by the magnitude of a momentum thickness Reynolds number specified in the program input. In case of this project the laminar turbulent transition momentum thickness Reynolds number was set to be 275. This value was chosen to correspond to experimental observations for a zero pressure gradient flow.

The Reynolds stress in the program is modelled using a Prandtl mixing-length scheme. The mixing-length is specified by a Van Driest exponential damping function for calculation of the

sublayer near the wall. In the model the viscous sublayer thickness, A^+, is 25 and von Karman constant, κ, is 0.41.

STANCOOL :

The prediction program STANCOOL is used to predict heat transfer in boundary layers with film cooling. The original program is described by Crawford,et al. (1980) and was derived from STAN5 to include the effects of film cooling. The program was developed especially for full coverage film cooling on flat isothermal surfaces.

The model used in the program simply modifies mass flow rate, velocity, and momentum of the flow at locations of injection. These parameters are modified in each streamtube. In the injection model of STANCOOL as a jet emerges into the boundary layer the shear layer at the injectant-boundary layer interface promotes entrainment of boundary layer fluid into the jet and eventually the injectant becomes diffused into the existing boundary layer. Equations describing the injection model are obtained from one-dimensional mass, momentum, and thermal energy balances on the element of injectant bounded between two stream surfaces. This element is shown in Fig.13.

In the turbulence model of STANCOOL augmented Prandtl mixing-length is used because of jet-boundary layer interaction. Augmentation of the two-dimensional mixing-length is shown in Fig.14.

In the present study this scheme was used with some modifications. Since an injection test model which does not provide full coverage has been used in the experiments, the STANCOOL program was modified to take this geometrical difference into consideration. The program logic was first changed to take the present injection geometry into account. Secondly two constants used in the program were replaced by the ones corresponding to the present case. Namely the modified constants are ALAM, the outer layer length-scale constant and DELMR, the mass shed ratio.

In the predictions ALAM was taken to be 0.03 and 0.4 and DELMR was taken to be 0.4 and 0.5 for blowing ratios of 1.00 and 1.56, respectively. These values were adjusted to correspond to experimental results. Both constants show qualitative agreement with the correlations given by Crawford et al. for full-coverage film cooling. Viscous sublayer thickness, A^+, was taken to be 22 in the cooled region to consider surface roughness due to holes.

7. RESULTS AND DISCUSSION

As mentioned before, the investigation of the effect of secondary flows and varible injection rate on heat transfer on a turbine endwall is the main purpose of this project. In order to achieve this goal, comparison of flat plate results with turbine endwall results was necessary. Such a comparison is possible only if a common base is provided on both test models. Therefore in the experiments inlet and outlet Mach numbers, injection ratios and coolant temperature parameters were adjusted to be about the same. Inlet and outlet Mach numbers are approximately 0.22 and 0.77 in flat plate test section and 0.325 and 0.785 in the cascade model. The blowing ratios are from 0.95 to 1.56 on flat plate and from 0.96 to 1.15 in the cascade. The temperature parameter is 0.95 for the cascade and ranges from 0.95 to 0.98 for the flat plate. The pressure distribution on the flat plate model with respect to the injection locations is in qualitative agreement with the pressure distribution in the cascade model. The distributions are shown in Fig.8.

In Fig.9 heat transfer distributions on a flat plate with and without pressure gradient are shown. The data were taken without boundary layer trip. On both data sets the laminar-turbulent transition region is clearly observed. The transition region is approximately 65 mm away from the leading edge. The predictions of both cases are also included in this figure. STAN5 prediction scheme was used for both cases with a momentum thickness Reynolds number of 275 for transition. Good agreement exists between the data and the predictions for the zero-pressure gradient case. The match of laminar, transition, and turbulent zones can be observed for this case. Small differences between predictions and data are evident for the pressure gradient case.

Fig.10 contains heat transfer data taken on a flat plate with film cooling. On this figure two sets of film cooled flat plate data are shown together with the data without film cooling. Injection locations are shown on the figure. In these experiments there is a trip located 15 mm downstream of the leading edge as shown in Fig.4.

The effect of film cooling can be seen clearly on Fig.10. A large drop in heat transfer takes place downstream of

the injection locations. In this figure three data sets corresponding to blowing ratios of 0.0, 0.95, and 1.56 are given to show the effect of injection rate on heat transfer. From the figure, low heat transfer exists at high blowing ratios at a given location.

The predictions of the measurements taken with film cooling were attempted for two blowing ratios, 1.0 and 1.56, as illustrated on Fig.10. Even though the predictions and measurements are not in good quantitative agreement for these cases, they have the same qualitative trend. The figure shows that the effect of injection can be predicted and there is a qualitative agreement between measurements and predictions. A better agreement can be achieved by accurate determination of the constants of the prediction scheme which are ALAM and DELMR as mentioned before.

One set of the endwall heat transfer data is given in Fig.11 for comparison with flat plate results. This data set contains only the data taken by the heat transfer gages located along the center streamline whose location was calculated by Martensen method and shown in Fig.8 as the fourth streamline. The gages used for these measurements are 52,55,24,22,13,4,38,35,29,56,64,80,48 on Fig.5 and Fig.6. The injection locations are also shown on the figure. Although the effect of film cooling in both cases is obvious on the figure, no great quantitative differences between flat plate and endwall results are present. The results have the same magnitudes and an overall qualitative match of the two cases is evident. One may conclude from this figure that at least along the center streamline, the effect of three-dimensionality on heat transfer coefficient is small.

The two data points shown on the figure which were taken by gages 52 and 55 located in the uncooled upstream region can be accepted as two bad data points. This is because although these points are in uncooled region and out of the blade passage they have values different than flat plate measurements taken around corresponding locations. In this region values near to flat plate results would be more meaningful since this part of the cascade model is similar to a flat plate, and the existance of a two-dimensional boundary layer is expected.

On Fig.12 the effect of injection rate on endwall heat

transfer is shown. The results are again obtained along the center streamline of the cascade passage. The numbers of the gages used are 52,55,24,22,13 4,38,35,29,56,64,80,48. On the figure the effect of injection rate is evident. The lowest heat transfer coefficient corressponds to the highest blowing ratio of 1.15. The first two data points should again be accepted as bad data points, even though the measurements are repeatable at this location.

Table 2 contains the overall endwall heat transfer data at three injection ratios of 0.96, 1.00, and 1.15. When these data are investigated it is found that due to the secondary flow effects heat transfer distributions become very complex. The effects of secondary flow mechanisms shown in Fig.3 are observed. Analysis of the data sets shows that generally heat flux near the suction side is higher than the heat flux near the pressure side. One essential reason for this is the crossflow existing in the passage which is named as Crossflow A on Fig.3. Because of crossflow, injected cooling fluid is moved towards the suction side and heat transfer in this region becomes lower.

On the other hand, along a band located between the leading edge of one blade and the trailing edge of the opposite blade the heat flux is higher with respect to other regions. The measurements taken by gages 23,19,16,20,17,10,11,3,34,28,41,38,32,30 and 29 show this behaviour. This is also an expected trend because in this region, the passage vortex is present as shown in Fig.3.

On the suction side of the leading edge a hot region is present, as indicated by gage 8. In this region the counter vortex is present near the endwall. In the region where counter vortex is expected to lift off the endwall, this hot region disappears.

8. CONCLUSIONS

1. Flat plate measurements without injection show agreement with predictions providing a baseline check on measurement procedure.

2. Stanton numbers measured with film cooling show expected behaviour as the injection rate is changed.

3. Predictions of flat plate heat transfer with film cooling show qualitative agreement with measurements.

4. The hydrodynamic flow behaviour near the turbine endwall and in the turbine blade passage has been sketched from flow visualisations of secondary flow behaviour.

5. The heat transfer measured on the center streamline of the endwall with film cooling shows qualitative agreement with flat plate results.

6. The secondary flows near the turbine endwall cause non-uniform distributions of film cooling injectant resulting in varying heat transfer rates across the width of the passage.

REFERENCES

1. BLAIR,M.F.,"An Experimental Study of Heat Transfer and Film Cooling on Large Scale Turbine Endwalls" , ASME J. of Heat Transfer,Nov. 1974,pp. 524-529.

2. BLAIR,M.F.,"Investigation of Factors Affecting Heat Transfer to Turbine Endwalls",UARL Report L911324 Dec. 1972.

3. BOOTH,T.C.,"An Analysis of the Turbine Endwall Boundary Layer and Aerodynamic Losses",ASME Paper 75-GT-23,1975.

4. CAMCI,C.,LIGRANI,P.M.,HAY,N.,"Investigation of Heat Transfer Rates on a Film Cooled Flat Plate With and Without a Pressure Gradient",V.K.I.,Project report 1980-12,June 1980.

5. CONSIGNY,H.,CHAN,C.K.,RICHARDS,B.E.,"The Effect of Pressure Gradient and External Turbulence on Heat Transfer to a Cold Flat Plate",V.K.I.,TN 128,Feb. 1979.

6. CRAWFORD,M.E.,KAYS,W.M.,"STAN5-A Program for Numerical Computation of Two-Dimensional Internal and External Boundary Layer Flows",NASA CR-2742,Dec. 1976.

7. CRAWFORD,M.E.,KAYS,W.M.,MOFFAT,R.J.,"Heat Transfer with Full Coverage Film Cooling Using 30-Deg Slant Angle Injection",ASME Paper 75-WA/HT-11,1976.

8. DRING,R.P.,"A Momentum Integral Analysis of the Three Dimensional Turbine Endwall Boundary Layer",ASME Paper 71-GT-6,1971.

9. GEORGIOU,D.P.,GODARD,M.,RICHARDS,B.E.,"Experimental Study of the Iso-Heat-Transfer-Rate Lines on the Endwall of a Turbine Cascade",ASME Paper 79-GT-20,1979.

10. GRAZIANI,R.A.,BLAIR,M.F.,TAYLOR,J.R.,MAYLE,R.E., "An Experimental Study of Endwall and Airfoil Surface Heat Transfer in a Large Scale Turbine Blade Cascade" ASME J. of Engineering for Power,April 1980,pp.257-267.

11. LANGSTON,L.S.,"Crossflows in a Turbine Cascade Passage" ASME Paper 80-GT-5,1980.

12. LANGSTON,L.S.,NICE,M.L.,HOOPER,R.M.,"Three-Dimensinal Flow Within a Turbine Cascade Passage",ASME Paper 76-GT-50,1976.

13. LIGRANI,P.M.,BREUGELMANS,F.A.E.,"Turbine Blade Cooling Research at the von Karman Institute for Fluid Dynamics," Fifth International Symposium on Air Breathing Engines,Feb. 16-21,1981,Bangalore,India.

14. LOUIS,J.F.,GOULIOS,G.N.,DEMIRJIAN,A.M.,TOPPING,R.F., and WIEDHOPF,J.M.,"Short Duration Studies of Turbine Heat Transfer and Film Cooling Effectiveness",ASME Paper 74-GT-131,1974.

15. MARCHAL,Ph.,and SIEVERDING,C.H.,"Secondary Flow Within Turbine Bladings",AGARD-CPP-214,Secondary Flows in Turbomachines,March 1977,Netherlands.

16. PATANKAR,S.V. and SPALDING,D.B.,"Heat and Mass Transfer in Boundary Layers,2nd Ed.,International Textbook Company Ltd.,London,1970.

17. SIEVERDING,C.H.,and WILPUTTE,Ph.,"Influence of Mach Number and Endwall Cooling on Secondary Flows in a Straight Nozzle Cascade",ASME Paper 80-GT-52,1980.

18. SCHULTZ,D.L.,and JONES,T.V.,"Heat Transfer Measurements in Short Duration Hypersonic Facilities", AGARDOGRAPH No: 165,Feb. 1973.

19. VAN DEN BRAEMBUSSCHE,R.A.,"Calculation of Compressible Subsonic Flow in Cascades with Varying Blade Height", ASME Paper 73-GT-59,April 1973.

20. VILLE,J.P.,GODARD,M.,RICHARDS,B.E.,and SIEVERDING,C.H., "Film Cooling and Endwall Heat Transfer in Small Turbine Blade Passages",V.K.I.,TN 126,Feb. 1978.

21. WHITNEY,W.J.,SZANCA,E.M.,MOFFITT,T.P.,and MONROE,D.E., "Cold Air Investigation of a Turbine for High Temperature Engine Application",Part 1,NASA TN D-3751,1967.

22. CRAWFORD,M.E.,KAYS,W.M.,and MOFFAT,R.J.,"Full-Coverage Film Cooling on Flat Isothermal Surfaces : A Summary Report on Data and Predictions",NASA CR-3219, NAS3-14336, Jan. 1980.

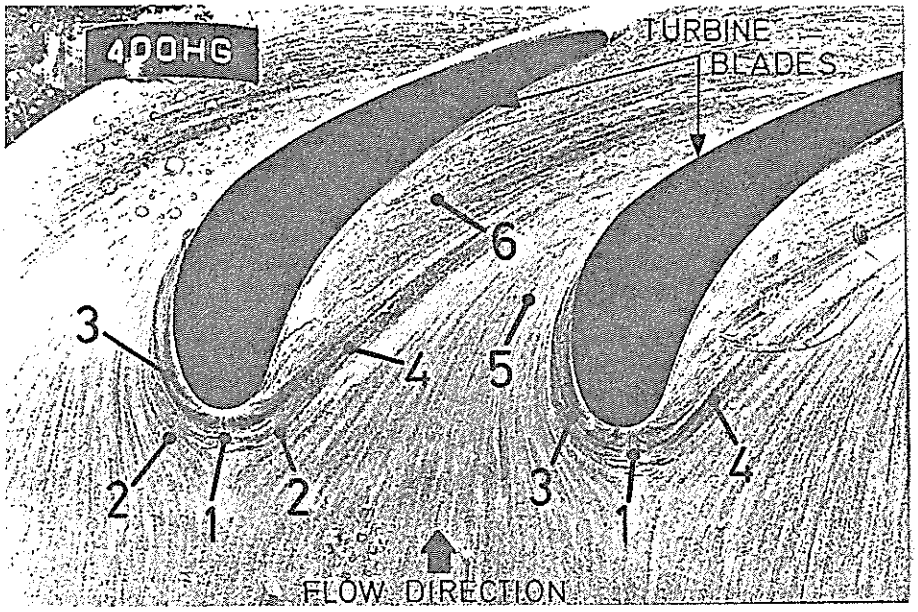

1- SADDLE POINT

2- SEPARATION LINE OF INLET BOUNDARY LAYER

3- ENDWALL SEPARATION LINE OF COUNTER VORTEX

4- ENDWALL SEPARATION LINE OF PASSAGE VORTEX

5- CROSSFLOW A

6- CROSSFLOW B

FIG. 1 – OIL FLOW VISUALIZATION OF TURBINE CASCADE ENDWALL FLOW

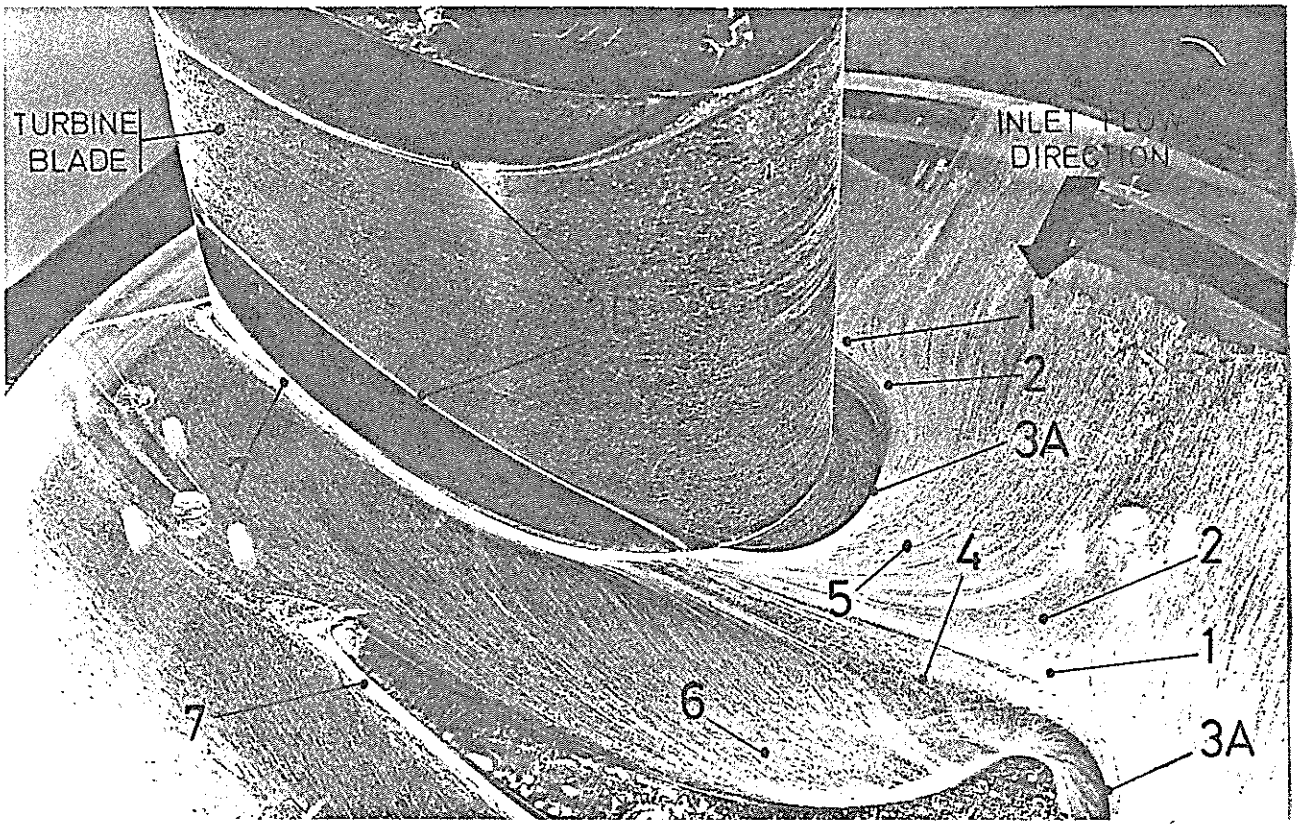

1– SADDLE POINT

2– SEPARATION LINE OF INLET BOUNDARY LAYER

3A–ENDWALL SEPARATION LINE OF COUNTER VORTEX

3B–BLADE SEPARATION LINE OF COUNTER VORTEX

4– ENDWALL SEPARATION LINE OF PASSAGE VORTEX

5– CROSSFLOW A

6– CROSSFLOW B

7– SEPARATION LINE OF CORNER VORTEX

FIG. 2– OIL FLOW VISUALISATION OF FLOW OVER TURBINE CASCADE ENDWALL AND TURBINE BLADE

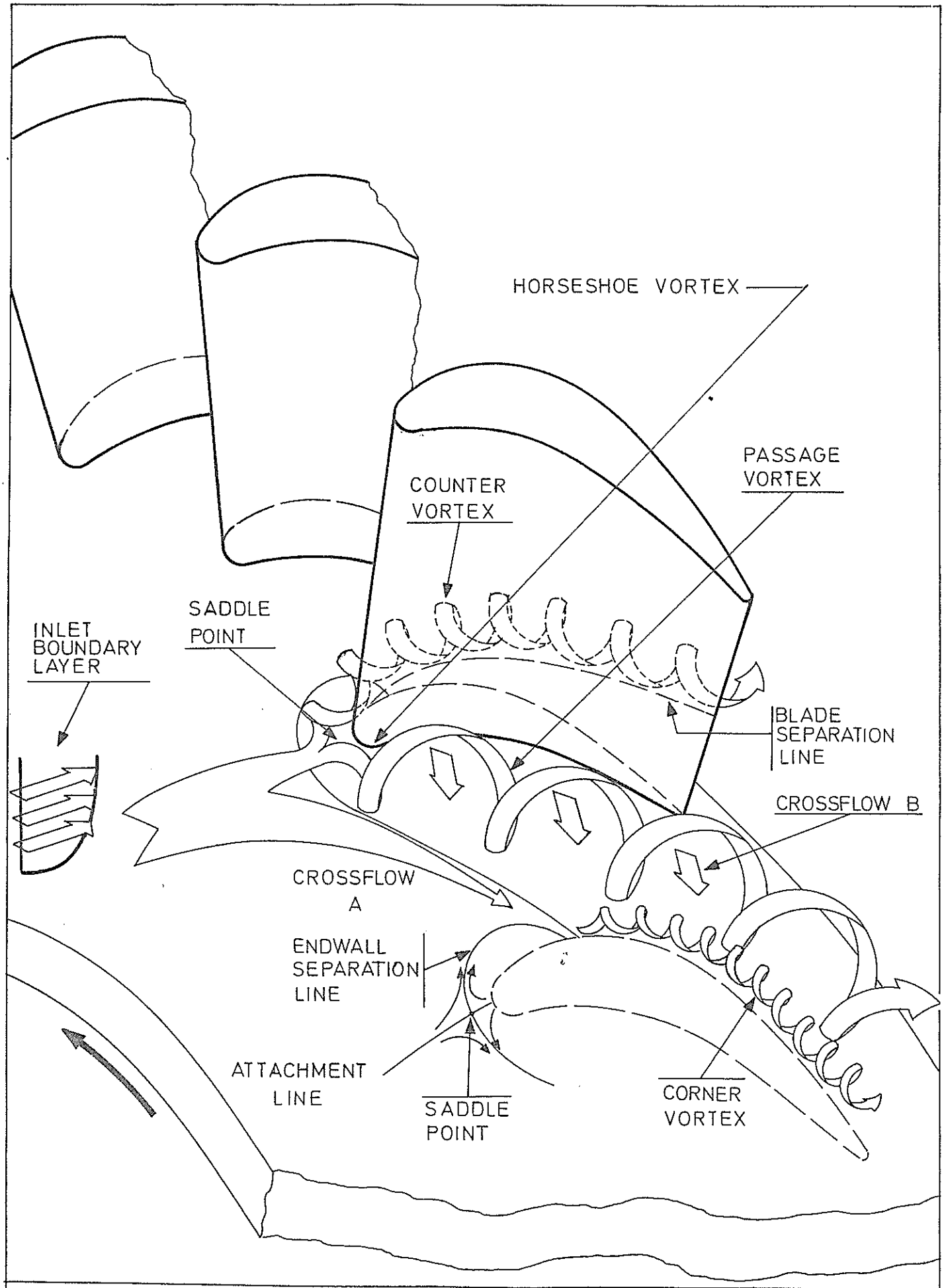

FIG. 3 — ENDWALL SECONDARY FLOWS

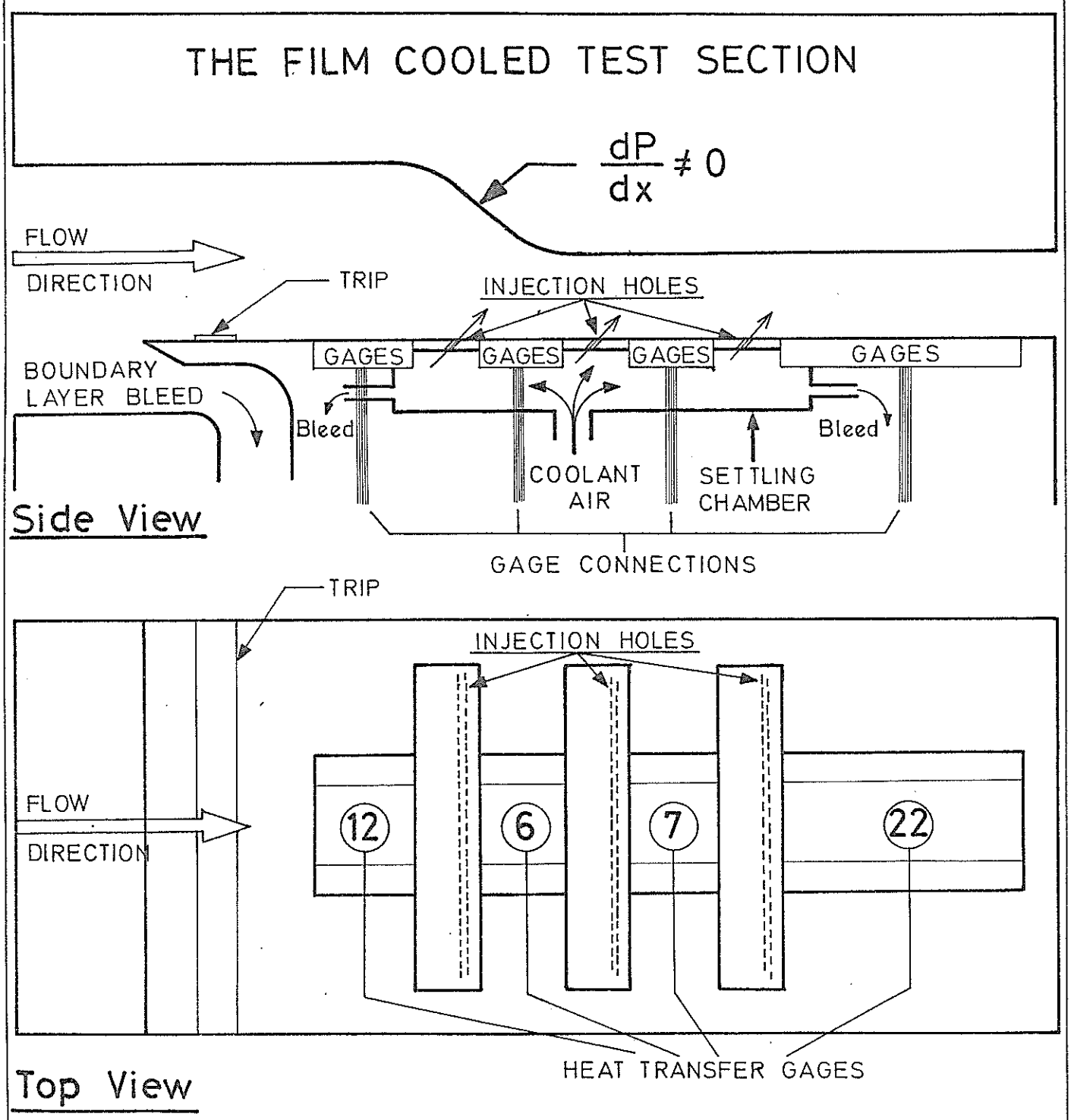

FIG.4 – THE SKETCH OF FLAT PLATE TEST SECTION

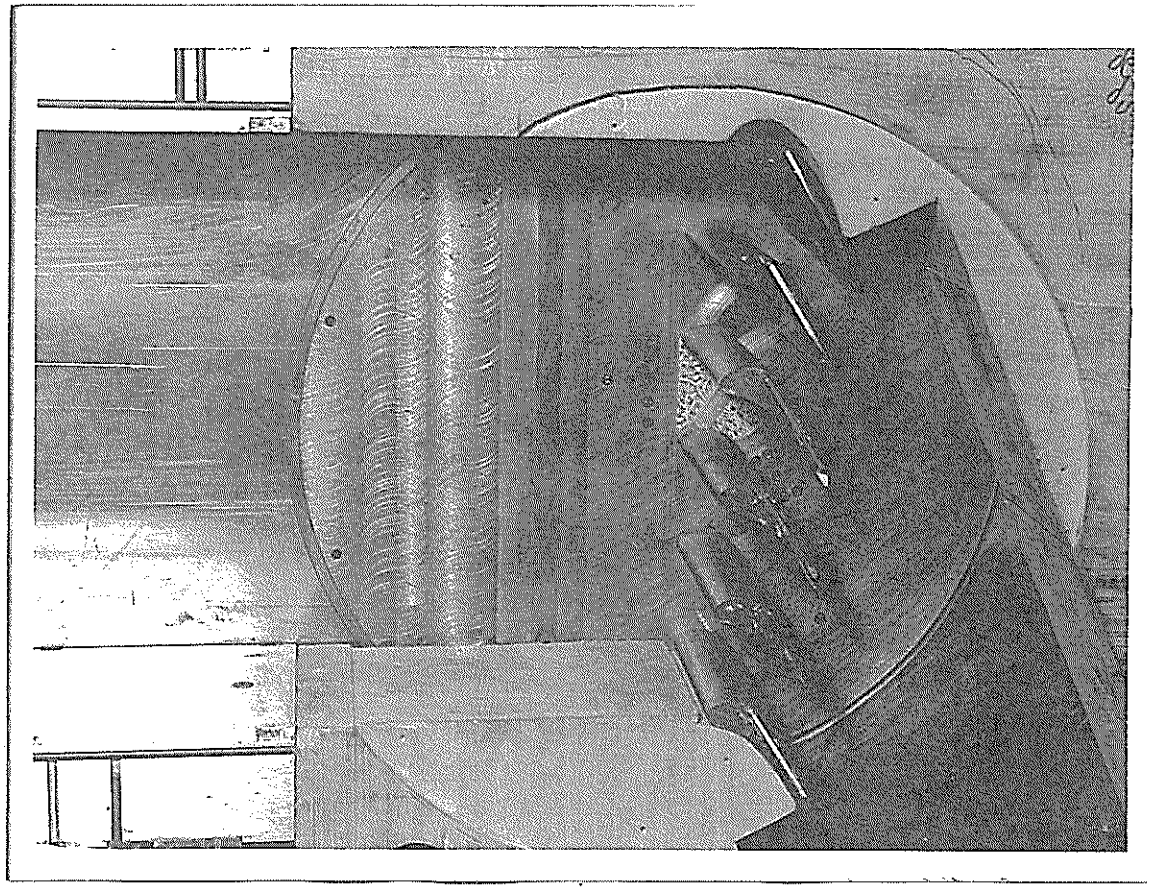

PLATE 2 — ENDWALL MODEL IN THE TEST SECTION

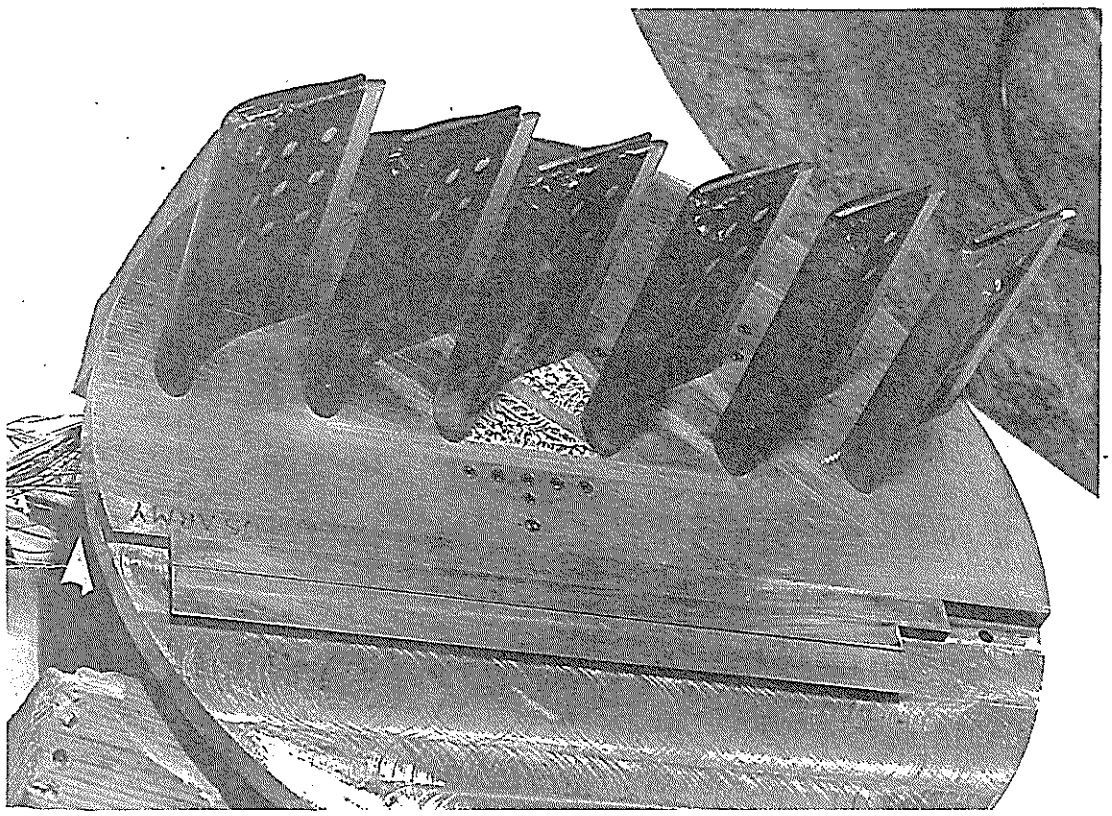

PLATE 1 — ENDWALL MODEL WITH BLADES

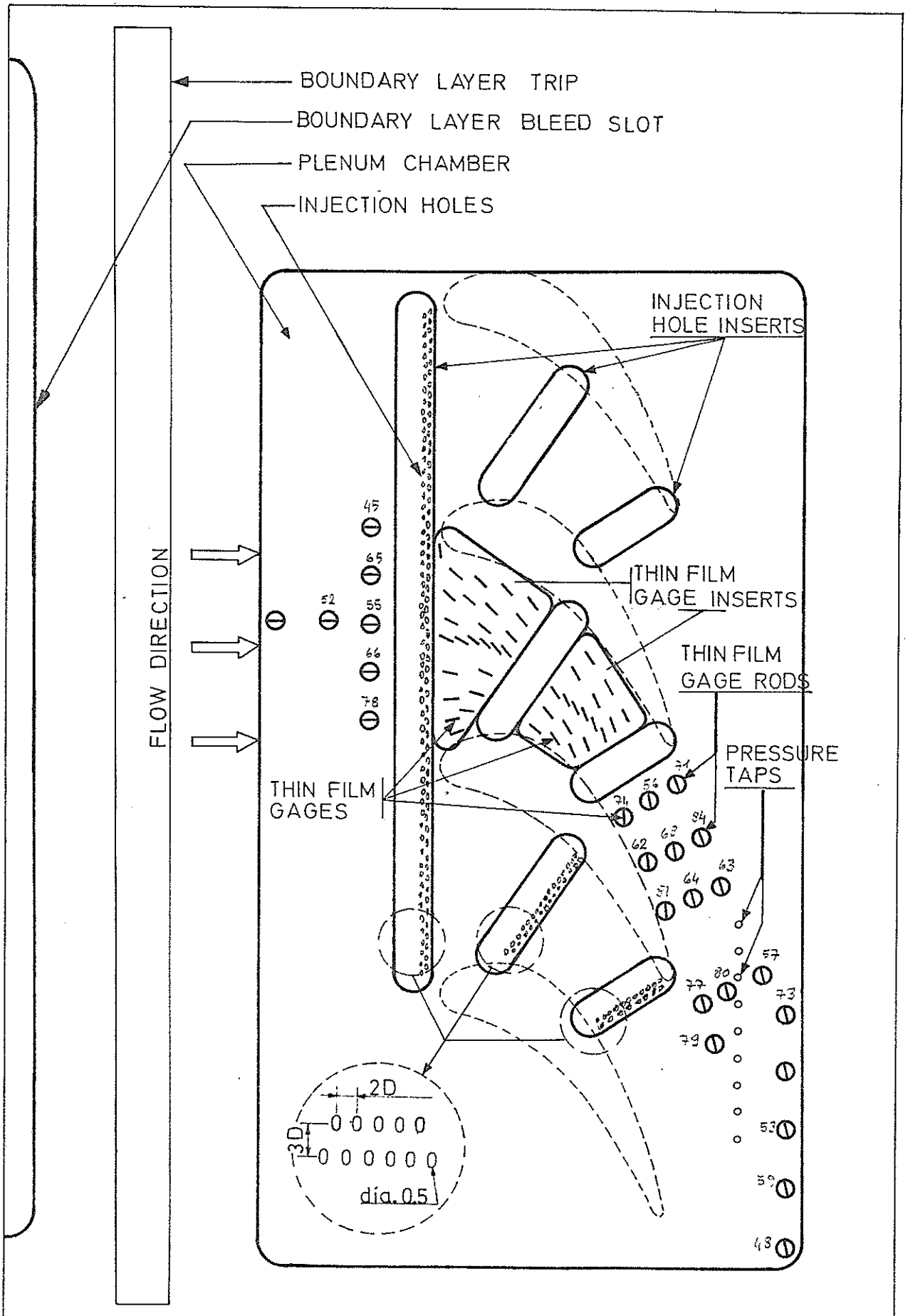

FIG. 5 – ENDWALL INJECTION HOLE AND THIN FILM GAGE ORIENTATION

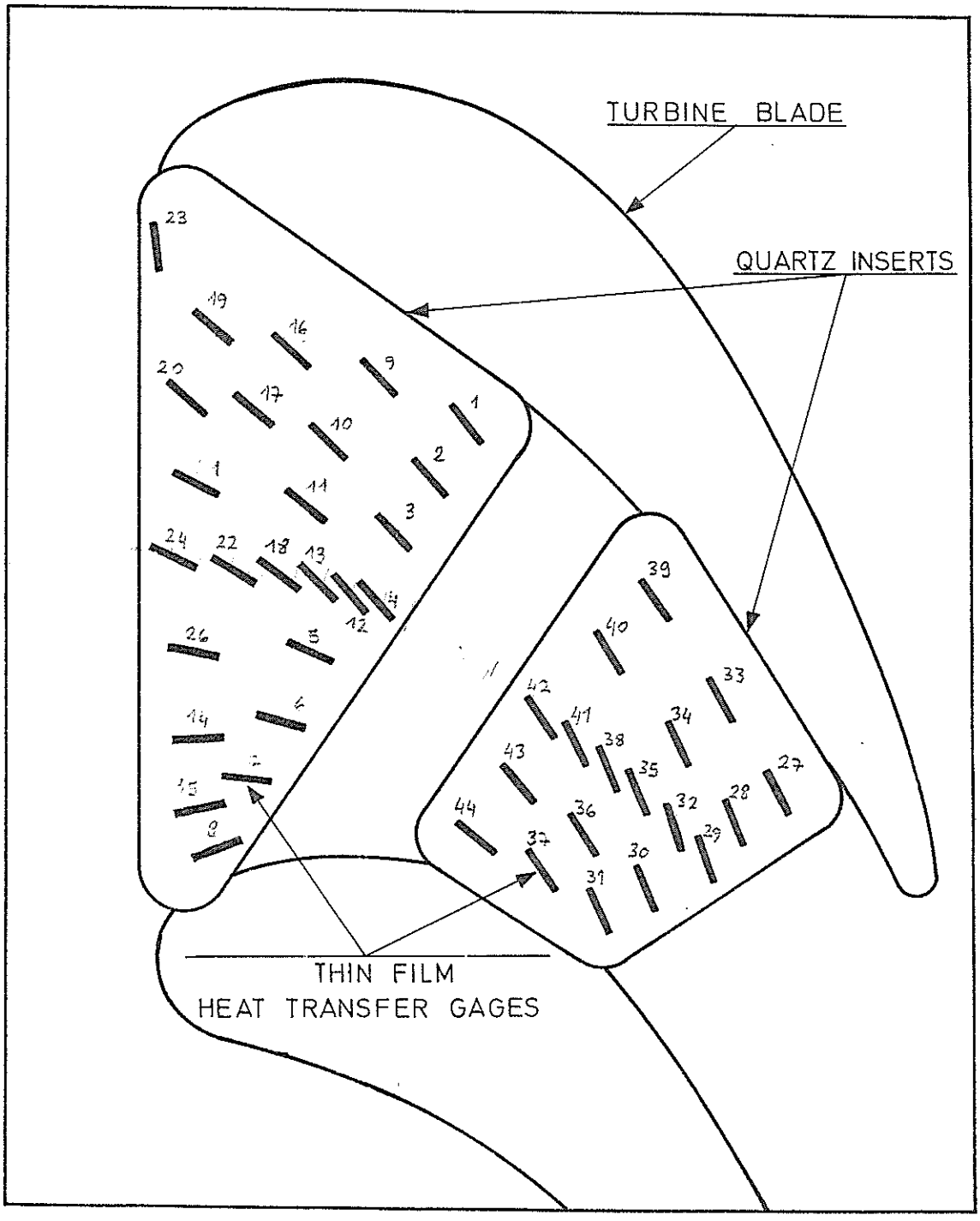

FIG. 6 – THIN FILM GAGE ORIENTATION ON QUARTZ INSERTS

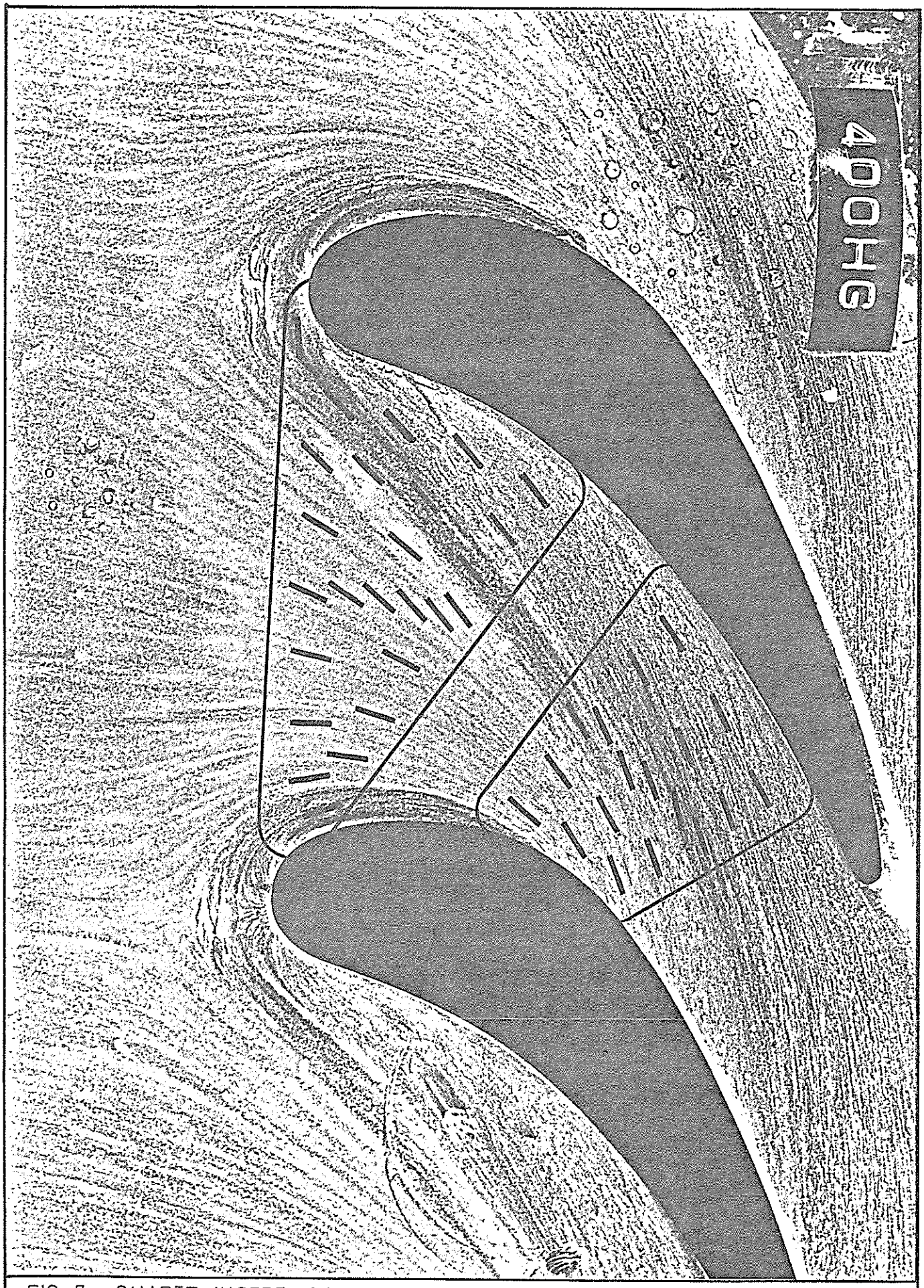

FIG. 7 – QUARTZ INSERT GAGE ORIENTATION AND ENDWALL FLOW VISUALIZATION

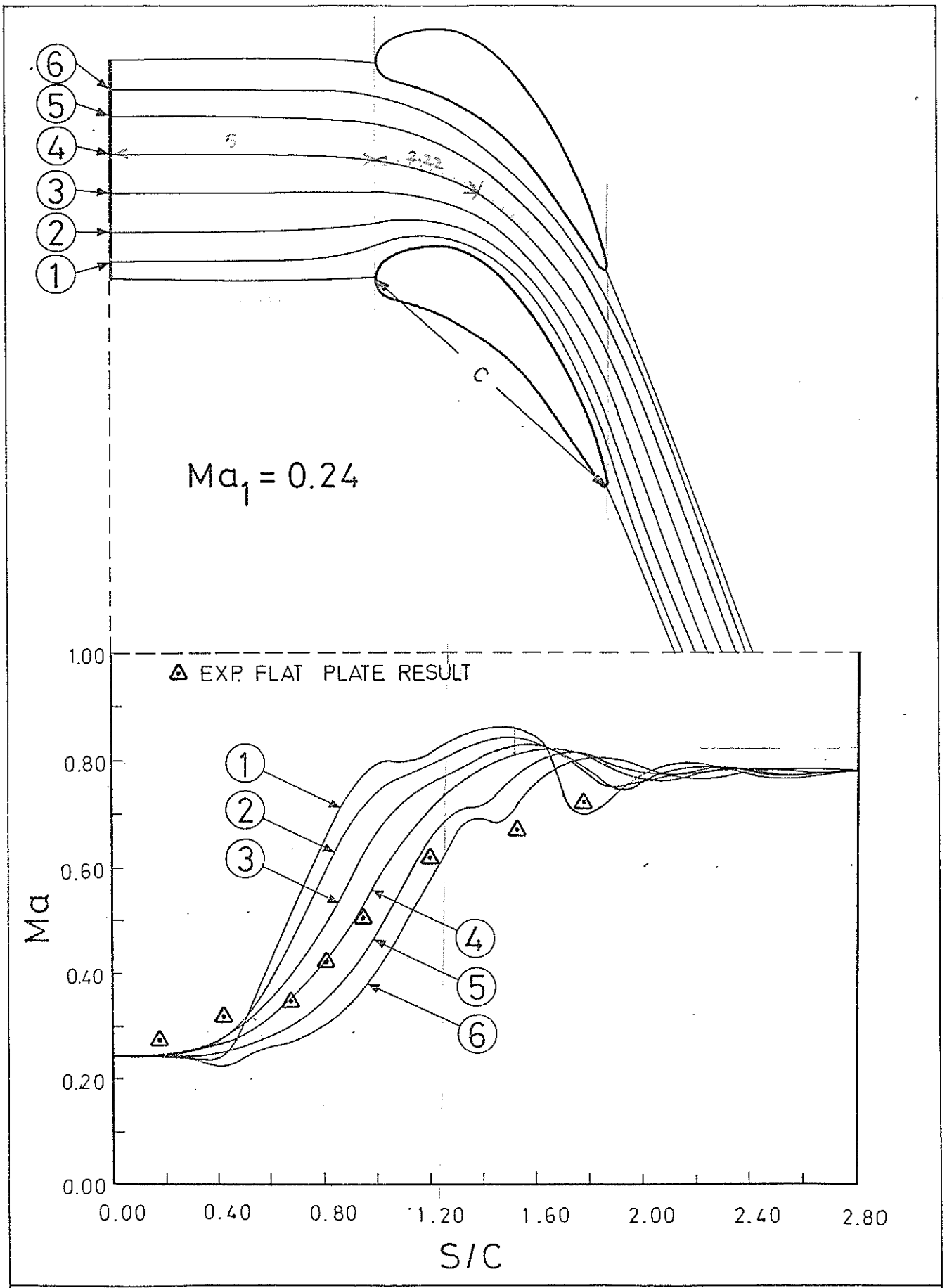

FIG. 8 - STREAMLINES AND CALCULATED MACH NUMBER DISTRIBUTIONS IN CASCADE TEST SECTION

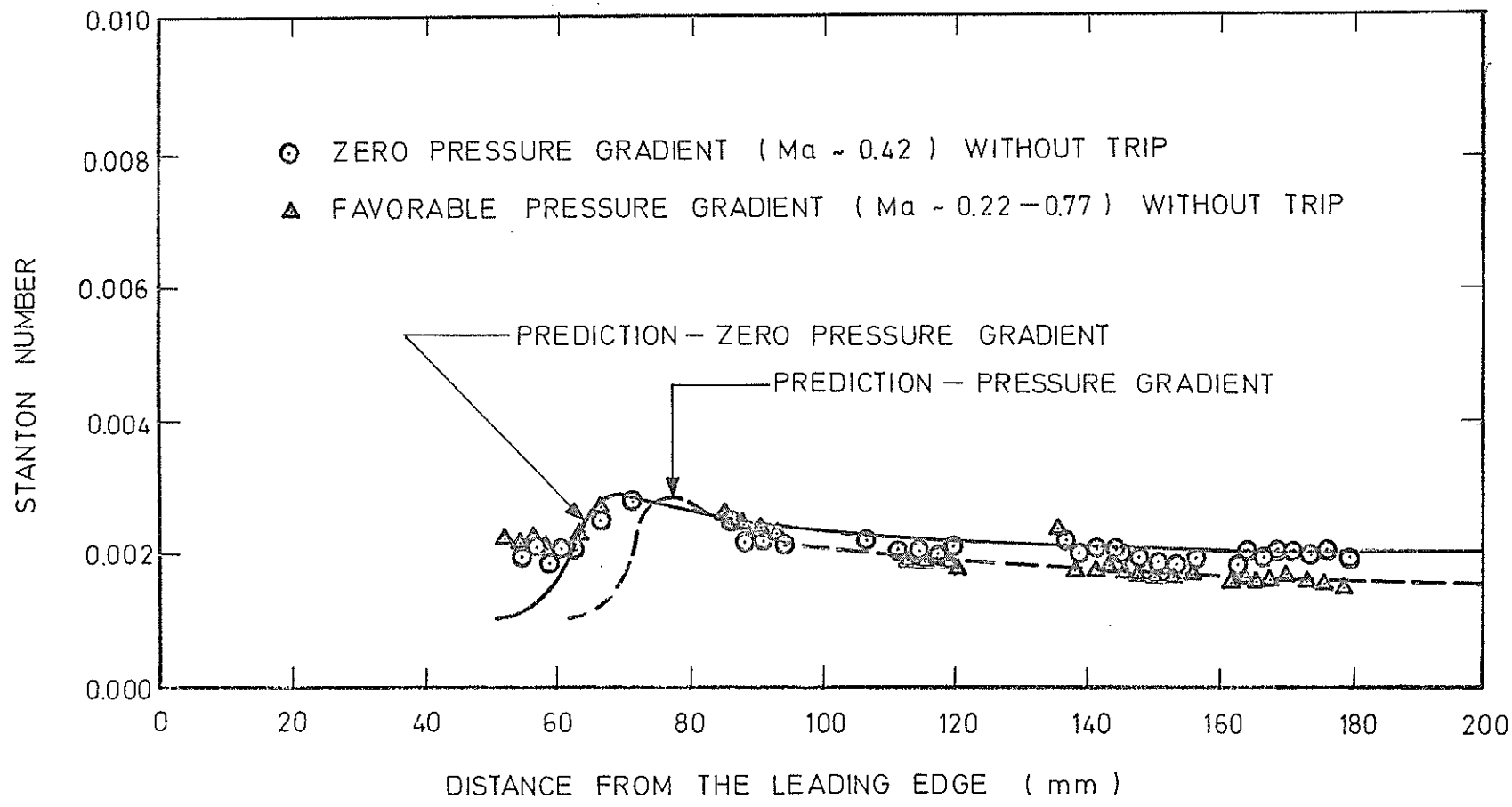

FIG. 9: – STANTON NUMBER DISTRIBUTIONS OVER A FLAT PLATE WITH AND WITHOUT PRESSURE GRADIENT

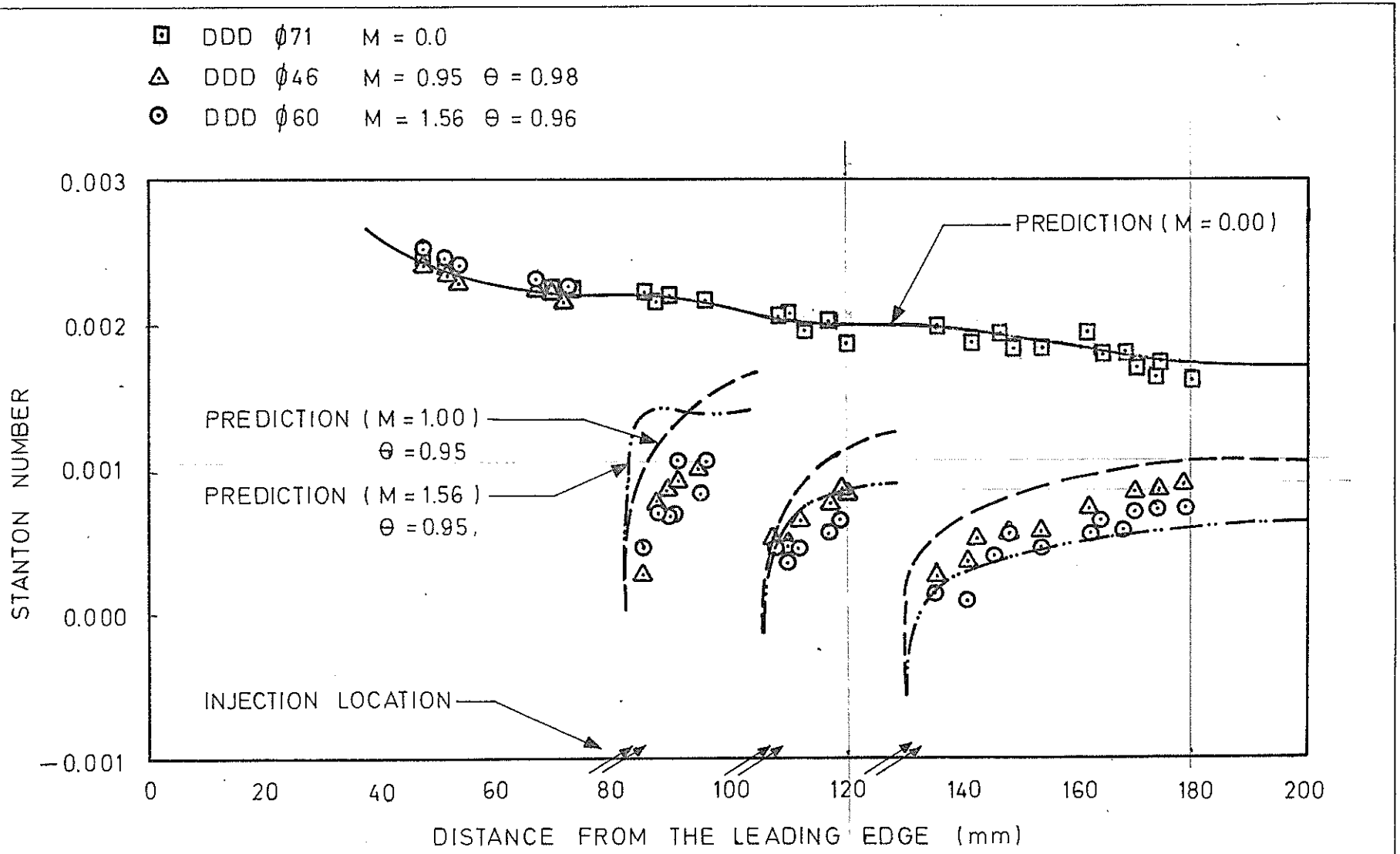

FIG.10 EFFECT OE VARIABLE INJECTION RATE ON STANTON NUMBERS ON A FLAT PLATE WITH PRESSURE GRADIENT AT CONSTANT INJECTION TEMPERATURE

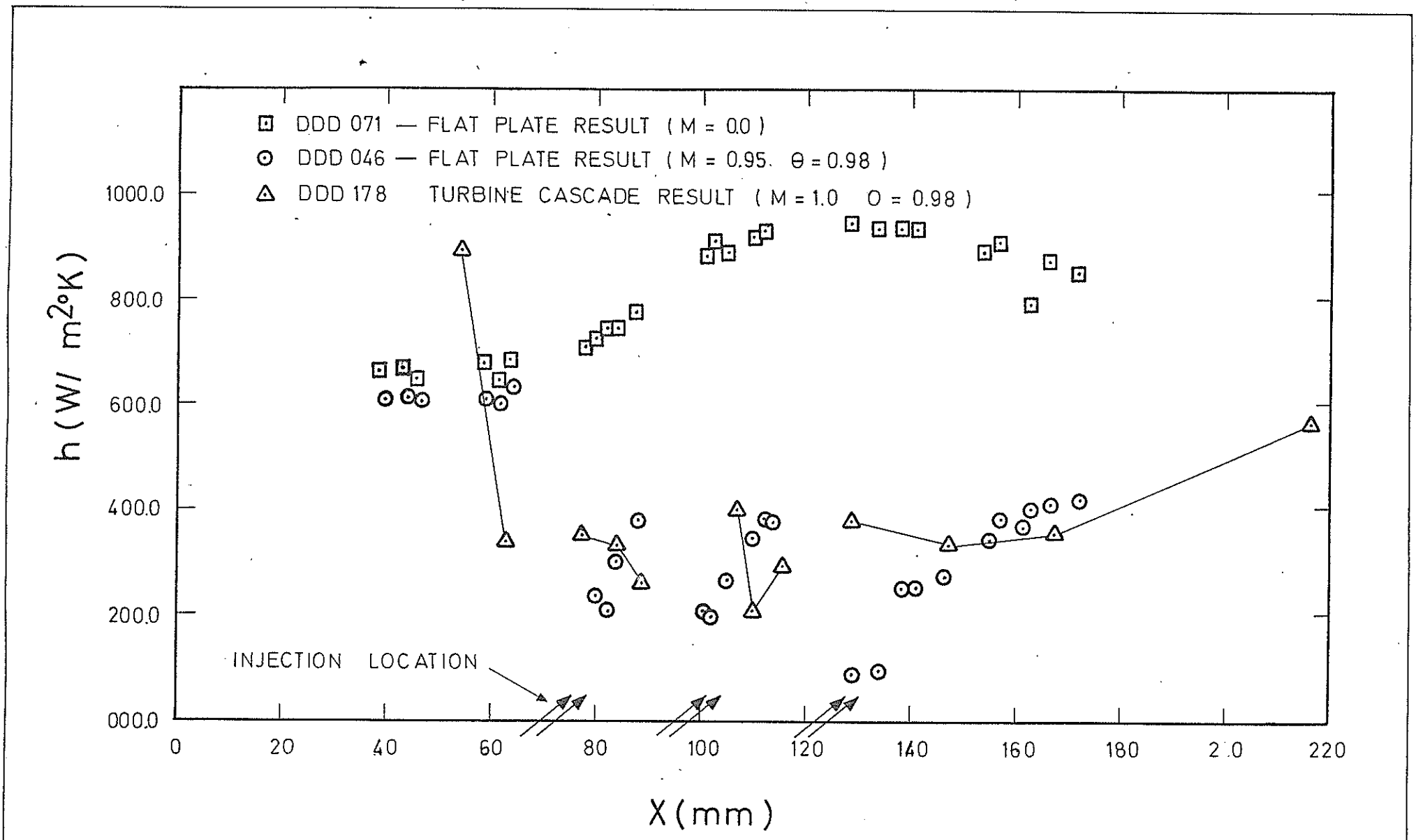

FIG. 11 COMPARISON OF FLAT PLATE HEAT TRANSFER RESULTS WITH TURBINE ENDWALL HEAT TRANFER RESULTS ALONG THE CENTER STREAMLINE.

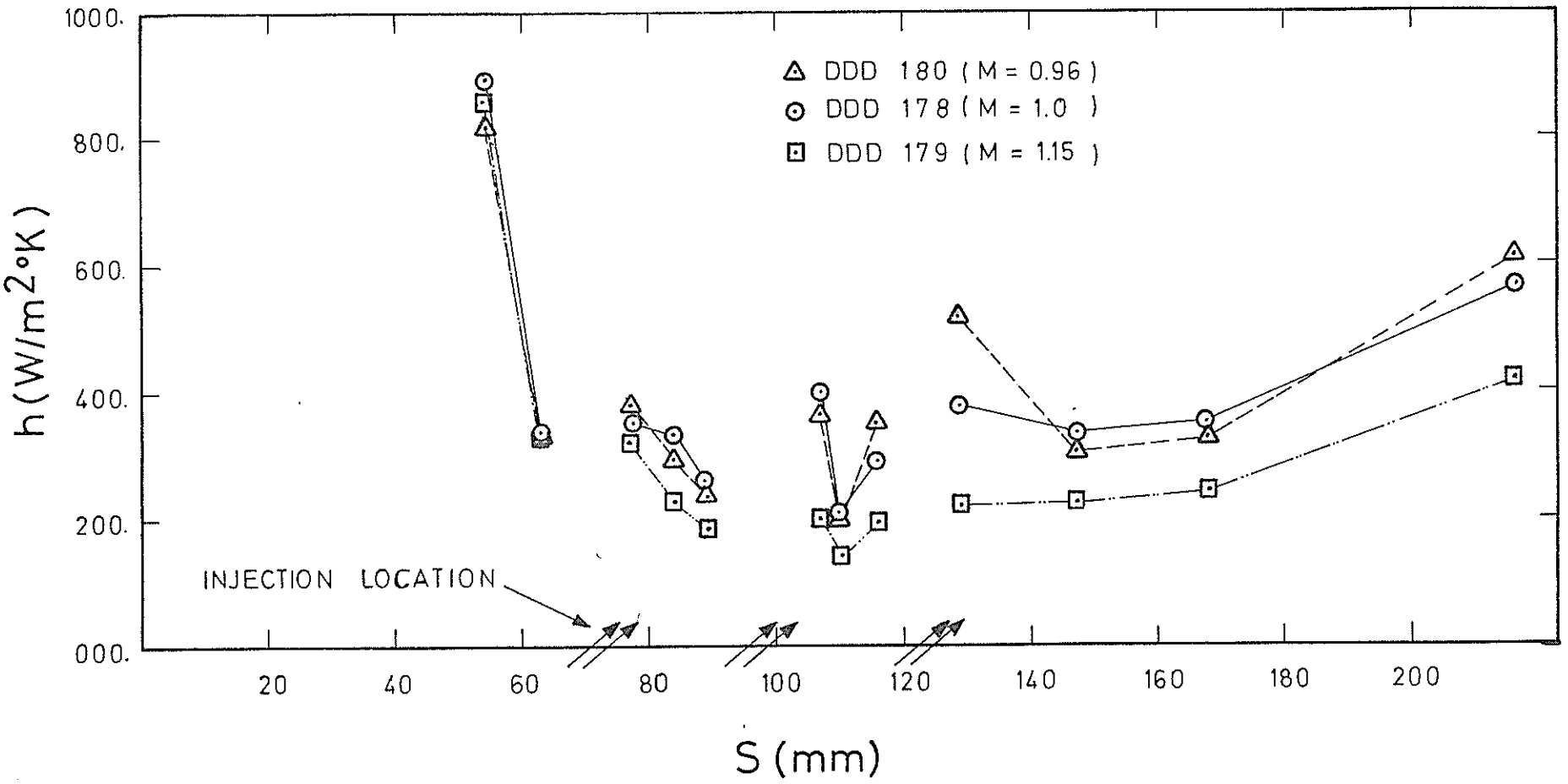

FIG. 12 EFFECT OF VARIABLE INJECTION RATE ON HEAT TRANSFER ON A TURBINE ENDWALL AT CONSTANT INJECTION TEMPERATURE

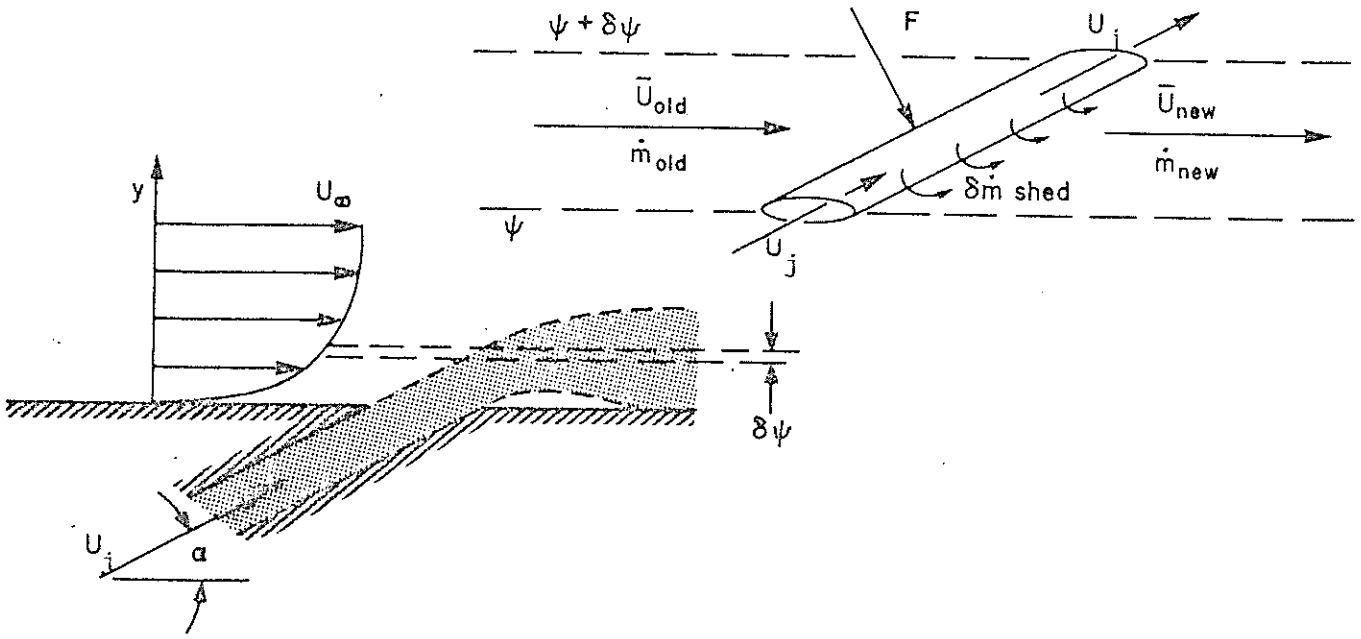

Fig. 13. Idealized representation of the injection process. (Ref. 7)

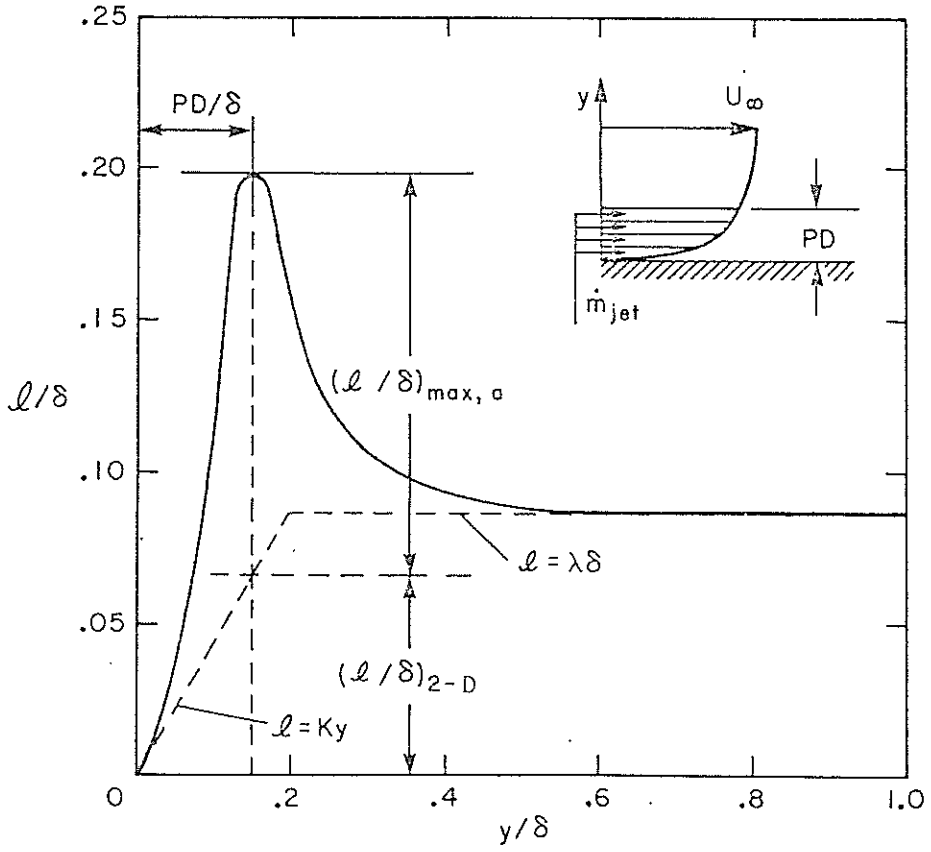

Fig. 14. Idealized representation of the distribution of mixing length in a full-coverge region. (Ref. 7)

	RUN NO : DDH 178		RUN NO : DDH 179		RUN NO : DDH 180	
GAGE NO.	Q (W/cm²)	h (W/m² °K)	Q (W/cm²)	h (W/m² °K)	Q (W/cm²)	h (W/m² °K)
52	0.950E+01	0.897E+03	0.914E+01	0.860 E+03	0.877E+01	0.823 E 03
55	0.361E+01	0.339E+03	0.353E+01	0.329 E+03	0.360E+01	0.339 E 03
24	0.377E+01	0.354E+03	0.345E+01	0.322 E+03	0.409E+01	0. 382 E 03
22	0.470E+01	0.447E+03	0.833E+01	0.786 E+03	0.771E+01	0. 730 E 03
43	0.351E+01	0.329E+03	0.245E+01	0. 228 E+03	0.315E+01	0. 295 E 03
4	0.287E+01	0.270E+03	0.199E+01	0. 185 E+03	0.253E+01	0. 237 E 03
41	0.842E+01	0.794E+03	0.703E+01	0. 658 E+03	0.780E+01	0. 734 E 03
38	0.436E+01	0.409E+03	0.217E+01	0. 202 E+03	0.392E+01	0. 367 E 03
35	0.217E+01	0.204E+03	0.152E+01	0. 142 E+03	0.214E+01	0. 200 E 03
32	0.697E+01	0.658E+03	0.618E+01	0. 578 E+03	0.676E+01	0. 636 E 03
13	0.308E+01	0.289E+03	0.209E+01	0. 196 E+03	0.380E+01	0. 356 E 03
56	0.409E+01	0.385E+03	0.241E+01	0. 225 E+03	0.558E+01	0. 522 E 03
48	0.617E+01	0.582E+03	0.448E+01	0. 419 E+03	0.648E+01	0. 609 E 03
64	0.351E+01	0.330E+03	0.243E+01	0. 227 E+03	0.328E+01	0. 309 E 03
80	0.374E+01	0.351E+03	0.264E+01	0. 245 E+03	0.352E+01	0. 330 E 03
99	0.136E+02	0.129E+04	0.131E+02	0. 124 E+04	0.124E+02	0. 118 E 04
53	0.314E+01	0.294E+03	0.160E+01	0. 149 E+03	0.344E+01	0. 322 E 03
71	0.433E+01	0.406E+03	0.398E+01	0. 371 E+03	0.442E+01	0. 413 E 03
84	0.688E+02	0.703E+04	0.672E+02	0. 692 E+04	0.626E+02	0. 652 E 04
63	0.584E+01	0.548E+03	0.477E+01	0. 444 E+03	0.597E+01	0. 559 E 03
74	0.250E+01	0.235E+03	0.176E+01	0.	0.239E+01	0.
62	0.820E+01	0.774E+03	0.660E+01	0. 618 E+03	0.771E+01	0. 729 E 03
81	0.252E+01	0.236E+03	0.121E+01	0. 113 E+03	0.266E+01	0. 248 E 03
77	0.190E+01	0.179E+03	0.139E+01	0. 130 E+03	0.231E+01	0. 216 E 03
79	0.815E+01	0.771E+03	0.672E+01	0. 630 E+03	0.740E+01	0. 698 E 03
45	0.448E+01	0.421E+03	0.278E+01	0.259 E+03	0.447E+01	0. 419 E 03
65	0.297E+01	0.278E+03	0.276E+01	0. 259 E+03	0.289E+01	0. 271 E 03
66	0.112E+02	0.106E+04	0.109E+02	0. 103 E+03	0.103E+02	0. 978 E 03
78	0.302E+01	0.284E+03	0.263E+01	0. 245 E+03	0.273E+01	0. 256 E 03
21	0.371E+01	0.349E+03	0.168E+01	0. 156 E+03	0.383E+01	0. 353 E 03
11	0.681E+01	0.645E+03	0.665E+01	0. 625 E+03	0.617E+01	0. 583 E 03
3	0.335E+01	0.315E+03	0.219E+01	0. 204 E+03	0.303E+01	0. 288 E 03
28	0.343E+01	0.322E+03	0.233E+01	0. 216 E+03	0.306E+01	0. 286 E 03
25	0.112E+02	0.106E+04	0.835E+01	0. 784 E+03	0.119E+02	0. 112 E 04
36	0.369E+01	0.346E+03	0.419E+01	0. 391 E+03	0.437E+01	0. 403 E 03
30	0.192E+02	0.184E+04	0.184E+02	0. 195 E+04	0.184E+02	0. 197 E 03
20	0.105E+02	0.992E+03	0.818E+01	0. 771 E+03	0.990E+01	0. 934 E 03

TABLE 2

TABLE 2 (continued)

GAGE NO.	RUN NO: DDD 181 Q (W/m²)	RUN NO: DDD 181 h (W/cm² °K)	RUN NO: DDD 182 Q (W/m²)	RUN NO: DDD 182 h (W/cm² °K)	RUN NO: DDD 183 Q (W/m²)	RUN NO: DDD 183 h (W/cm² °K)
8	0.869E+01	0.815E+03	0.829E+01	0.782E+03	0.110E+02	0.104E+04
15	0.272E+01	0.253E+03	0.269E+01	0.253E+03	0.438E+01	0.412E+03
7	0.241E+01	0.225E+03	0.231E+01	0.217E+03	0.405E+01	0.380E+03
14	0.731E+01	0.684E+03	0.721E+01	0.679E+03	0.871E+01	0.821E+03
6	0.242E+01	0.226E+03	0.231E+01	0.217E+03	0.373E+01	0.350E+03
26	0.187E+01	0.174E+03	0.180E+01	0.169E+03	0.322E+01	0.302E+03
25	0.856E+01	0.802E+03	0.842E+01	0.794E+03	0.841E+01	0.793E+03
21	0.276E+01	0.257E+03	0.258E+01	0.242E+03	0.413E+01	0.388E+03
11	0.173E+01	0.161E+03	0.203E+01	0.190E+03	0.282E+01	0.264E+03
3	0.759E+01	0.711E+03	0.752E+01	0.709E+03	0.836E+01	0.788E+03
20	0.328E+01	0.305E+03	0.280E+01	0.263E+03	0.400E+01	0.375E+03
17	0.265E+01	0.248E+03	0.252E+01	0.237E+03	0.387E+01	0.364E+03
10	−0.593E−01	−0.552E+01	−0.224E+00	−0.210E+02	−0.255E+00	−0.240E+02
2	0.262E+01	0.244E+03	0.273E+01	0.256E+03	0.413E+01	0.388E+03
23	0.303E+01	0.282E+03	0.280E+01	0.263E+03	0.492E+01	0.462E+03
19	0.759E+01	0.710E+03	0.722E+01	0.681E+03	0.849E+01	0.800E+03
16	0.244E+01	0.227E+03	0.230E+01	0.216E+03	0.324E+01	0.304E+03
9	0.268E+01	0.249E+03	0.265E+01	0.248E+03	0.403E+01	0.379E+03
1	0.655E+02	0.660E+04	0.643E+02	0.641E+04	0.654E+02	0.660E+04
44	0.273E+01	0.254E+03	0.292E+01	0.274E+03	0.489E+01	0.459E+03
37	0.111E+01	0.104E+03	0.122E+01	0.114E+03	0.223E+01	0.209E+03
31	0.621E+01	0.581E+03	0.623E+01	0.588E+03	0.780E+01	0.736E+03
36	0.157E+01	0.147E+03	0.168E+01	0.158E+03	0.255E+01	0.239E+03
30	0.264E+01	0.246E+03	0.275E+01	0.258E+03	0.466E+01	0.438E+03
28	0.602E+01	0.563E+03	0.639E+01	0.602E+03	0.823E+01	0.776E+03
33	−0.145E−02	−0.135E+00	−0.124E−02	−0.116E+00	−0.120E−02	−0.113E+00
33	0.458E+01	0.427E+03	0.494E+01	0.464E+03	0.566E+01	0.531E+03
27	0.136E+02	0.128E+04	0.139E+02	0.132E+04	0.141E+02	0.133E+04
68	0.116E+01	0.108E+03	0.151E+01	0.142E+03	0.234E+01	0.220E+03
52	0.457E+01	0.426E+03	0.455E+01	0.428E+03	0.450E+01	0.423E+03
55	0.145E+01	0.136E+03	0.144E+01	0.135E+03	0.144E+01	0.135E+03
24	0.428E+01	0.399E+03	0.388E+01	0.364E+03	0.469E+01	0.441E+03
22	−0.160E+01	−0.150E+03	−0.572E+01	−0.539E+03	0.513E+01	0.482E+03
13	0.896E+01	0.841E+03	0.872E+01	0.823E+03	0.977E+01	0.923E+03
4	0.429E+01	0.400E+03	0.417E+01	0.392E+03	0.533E+01	0.501E+03
41	0.230E+01	0.214E+03	0.261E+01	0.245E+03	0.372E+01	0.349E+03
38	0.138E+02	0.131E+04	0.136E+02	0.129E+04	0.140E+02	0.133E+04

TABLE 2 (Continued)

GAGE NO.	RUN NO: DHD 184 Q(W/m²)	RUN NO: DHD 184 h(W/cm² °K)	RUN NO: DHD 185 Q(W/m²)	RUN NO: DHD 185 h(W/cm² °K)
8	0.106E+02	0.100E+04	0.112E+02	0.105E+04
15	0.372E+01	0.349E+03	0.400E+01	0.372E+03
7	0.415E+01	0.390E+03	0.421E+01	0.392E+03
14	0.960E+01	0.906E+03	0.102E+02	0.953E+03
6	0.457E+01	0.429E+03	0.475E+01	0.442E+03
26	0.385E+01	0.362E+03	0.417E+01	0.389E+03
25	0.899E+01	0.848E+03	0.967E+01	0.905E+03
21	0.407E+01	0.382E+03	0.406E+01	0.378E+03
11	0.294E+01	0.276E+03	0.292E+01	0.272E+03
3	0.839E+01	0.791E+03	0.882E+01	0.825E+03
20	0.369E+01	0.347E+03	0.359E+01	0.335E+03
17	0.366E+01	0.345E+03	0.383E+01	0.357E+03
10	-0.374E+00	-0.352E+02	0.718E+00	0.669E+02
2	0.420E+01	0.395E+03	0.445E+01	0.414E+03
23	0.459E+01	0.431E+03	0.497E+01	0.463E+03
18	0.836E+01	0.789E+03	0.895E+01	0.838E+03
16	0.327E+01	0.307E+03	0.339E+01	0.315E+03
9	0.388E+01	0.364E+03	0.394E+01	0.367E+03
1	0.646E+02	0.647E+04	0.716E+02	0.720E+04
44	0.547E+01	0.513E+03	0.885E+01	0.824E+03
37	0.311E+01	0.292E+03	0.470E+01	0.438E+03
31	0.868E+01	0.819E+03	0.104E+02	0.973E+03
36	0.310E+01	0.291E+03	0.481E+01	0.448E+03
30	0.472E+01	0.443E+03	0.584E+01	0.544E+03
28	0.969E+01	0.914E+03	0.103E+02	0.966E+03
39	-0.115E-02	-0.108E+00	-0.128E-02	-0.119E+00
33	0.635E+01	0.596E+03	0.625E+01	0.582E+03
27	0.143E+02	0.135E+04	0.153E+02	0.143E+04
68	0.247E+01	0.232E+03	0.289E+01	0.269E+03
52	0.451E+01	0.423E+03	0.453E+01	0.422E+03
55	0.142E+01	0.134E+03	0.158E+01	0.147E+03
24	0.493E+01	0.463E+03	0.497E+01	0.463E+03
22	0.509E+01	0.478E+03	0.505E+01	0.471E+03
13	0.955E+01	0.902E+03	0.102E+02	0.960E+03
4	0.529E+01	0.498E+03	0.560E+01	0.522E+03
41	0.360E+01	0.339E+03	0.560E+01	0.521E+03
38	0.140E+02	0.133E+04	0.172E+02	0.162E+04

TABLE 2 (Continued)

CASE NO	q (W/m²)	h (W/m² °K)
52	0.969E+01	0.915E+03
55	0.503E+01	0.473E+03
24	0.497E+01	0.467E+03
22	0.141E+02	0.134E+04
13	0.370E+01	0.347E+03
4	0.361E+01	0.339E+03
41	0.986E+01	0.930E+03
38	0.521E+01	0.490E+03
35	0.531E+01	0.499E+03
32	0.690E+01	0.634E+03
29	0.117E+02	0.111E+04
56	0.419E+01	0.393E+03
48	0.861E+01	0.813E+03
64	0.382E+01	0.359E+03
80	0.641E+01	0.603E+03
57	0.163E+02	0.155E+04
59	0.593E+01	0.557E+03
71	0.478E+01	0.449E+03
84	0.735E+02	0.749E+04
63	0.607E+01	0.570E+03
74	0.215E+01	0.202E+03
62	0.641E+01	0.869E+03
81	0.345E+01	0.324E+03
72	0.128E+02	0.122E+04
73	0.863E+01	0.815E+03
45	0.296E+01	0.278E+03
65	0.233E+01	0.219E+03
66	0.124E+02	0.118E+04
78	0.486E+01	0.457E+03
21	0.433E+01	0.407E+03
11	0.442E+01	0.417E+03
3	0.364E+01	0.342E+03
28	0.639E+01	0.600E+03
25	0.109E+02	0.103E+04
36	0.394E-01	0.320E+04
20	0.560E+01	0.526E+03
10	0.123E+02	0.116E+04

APPENDIX A

CALCULATION OF THE FLOW CONDITIONS :

MASS FLOW RATE :

Calculation of the mass flow rate through the cascade model is made by the equation,

$$\dot{m}_p = \rho_p A_p U_p = \frac{P_p}{R T_p} M_p A_p (k R T_p)^{1/2} \qquad (1)$$

assuming isentropic expansion through the cascade. The air is taken to be a perfect gas in the calculations. Taking the cascade inlet Mach number as 0.24 we obtain from gas tables that($P_{o,p}/P_p$) and ($T_{o,p}/T_p$) are 1.041 and 1.012,respectively. From the given cascade geometry,

g/c = 0.725
c = 60 mm
h_c = 90 mm
n = number of passages = 5

Flow passage area can be written as,

$$A_p = (g/c)\, c\, h_c\, n\, b \qquad (2)$$

where b is the blokage factor and it is 0.7 in this case. Inserting above values into this equation gives,

$$A_p = 0.0137 \text{ m}^2$$

The cascade total pressure and temperature can be taken as the total pressure and temperature in front of the cascade which is 2.553 bars and 390 °K in the present case. Therefore,

P_p = 2.475
T_p = 385.4 °K

Then the mass flow rate is 2.895 kg/sec from the fist equation.

CASCADE FLOW RATE :

From the mass flow rate equation (Eq.1),

$$u_T A_T = (\dot{m}/\rho_p) = \frac{\dot{m}}{(P_T/RT_p)} \qquad (3)$$

Inserting the given values into this equation gives the flow rate as 1.2938 m^3/sec. The piston area of the compression tube is,

$$A_p = \pi D_p^2/4 = 0.7854 \ m^3$$

where the diameter of the tube is 1 meter.The tube length is 5 meters.

Assuming isentropic compression one can write,

$$\ell_2 = \ell_1 \left(\frac{P_1}{P_2}\right)^{1/k} \qquad (4)$$

Combining equation 3 and 4 yields,

$$t = \frac{\ell_2}{u_T} = \frac{\ell_1 \left(P_1/P_2\right)^{1/k}}{\dot{m}/(P_T/RT_p)} \cdot A_T \qquad (5)$$

where t is the compression time. Inserting the values for the unknowns gives for this case,

t = 1.5 sec

APPENDIX B

INJECTION SYSTEM DESIGN :

Double row of discrete hole injection system was used on the cascade test model. The injection holes are 30° slanted. Injection geometry is shown in Fig.5. The blowing ratio of the injection system is calculated by the expression,

$$M = \frac{\rho_c u_c}{\rho_\infty u_\infty} = (\alpha)^{2/\gamma}\left(\frac{T_\infty}{T_{o,c}}\right)^{1/2}\left[\frac{\left\{1-\left(\frac{\alpha P_o}{P_\infty}\right)^{-2/\gamma}\right\}}{\left\{1-\left(\frac{P_o}{P_\infty}\right)^{-2/\gamma}\right\}}\right]^{1/2} \qquad (1)$$

where,

$$\alpha = P_{o,c}/P_o$$

For given blowing ratio , coolant temperature, freestream total pressure and temperature and static pressure at the injection location , α value is calculated. Using this α value in the following expression,

$$\rho_c u_c = \rho_\infty \left(\frac{\alpha P_o}{P_\infty}\right)^{2/\gamma}\left[\frac{\gamma}{R T_{o,c}}\left\{1-\left(\frac{\alpha P_o}{P_\infty}\right)^{-2/\gamma}\right\}^{-2/\gamma}\right]^{1/2} \qquad (2)$$

coolant mass flow rate per unit area, $\rho_c u_c$, is obtained. The expression to be used in the ca-culation of coolant mass flow rate is

$$\dot{m}_c = \rho_c\, u_c\, A_c\, C_D \qquad (3)$$

where C_D is the discharge coefficient and it was taken to be 0.70 in the present case.

For the calculation of sonic orifice diameter Fleigner's formula is used. According to this formula the pressure upstream of the sonic orifice should be equal or greater than ($P_{o,c}$/0.528) in order to reach sonic conditions at the orifice. Keeping this in mind one can write,

$$\frac{\dot{m}_c}{A^*}\,\frac{(T_o)^{1/2}}{P_o} = 0.532 \qquad (4)$$

Here, $\dot{m}$ is in (lbm/sec), T_o is in °R, P_o is in (lbf/ft^2) and A^* is in ft^2. For the present case the flow conditions are:

$$P_o = 2.576 \text{ bars}$$
$$T_{o,c} = 293 \text{ °K}$$
$$T_o = 390 \text{ °K}$$

and the number of injection holes at the mid injection location is 50 where hole diameter is 0.5 mm. So total injection area is 9.8175 square millimeters. Mach number at the injection region can be obtained from Martensen calculation results on Fig.8. This value is 0.78 in this case. Under these conditions the final results given in Table 3 are obtained. To assure the sonic conditions at the orifice the smallest orifice diameter was chosen in the present set-up.

TABLE 3

M	Ma	P/P_o	P bar	α	P_{oc} bar	$\rho_c u_c$ kg/m sec	$\dot{m}$ kg/sec	A^* mm^2	D mm
0.7	0.78	1.495	1.723	0.788	2.030	352.44	2.442E-3	4.5818	2.418
1.0	0.78	1.495	1.723	o.917	2.362	505.03	3.470E-3	6.5800	2.894
1.3	0.78	1.495	1.723	1.10	2.834	659.73	4.534E-3	8.5955	3.308

Pg: 15
'ommon → common